JGR Atmospheres

RESEARCH ARTICLE
10.1029/2019JD031892

Toward a Reanalysis of Stratospheric Ozone for Trend Studies: Assimilation of the Aura Microwave Limb Sounder and Ozone Mapping and Profiler Suite Limb Profiler Data

Krzysztof Wargan[1,2], Natalya Kramarova[3], Brad Weir[4,2], Steven Pawson[2], and Sean M. Davis[5]

[1]Science Systems and Applications Inc., Lanham, MD, USA, [2]Global Modeling and Assimilation Office, Code 610.1, NASA Goddard Space Flight Center, Greenbelt, MD, USA, [3]Atmospheric Chemistry and Dynamics Lab, Code 614, NASA Goddard Space Flight Center, Greenbelt, MD, USA, [4]Universities Space Research Association, Columbia, MD, USA, [5]Chemical Sciences Division, NOAA Earth System Research Laboratory (ESRL), Boulder, CO, USA

Key Points:
- OMPS Limb Profiler stratospheric ozone data are assimilated into GEOS
- A simple homogenization method significantly reduces the bias between MLS and OMSP-LP ozone in assimilation
- Combined MLS and OMPS-LP data can provide continuity of ozone record in future reanalysis once the OMPS-LP drift problem is addressed

Correspondence to:
K. Wargan,
krzysztof.wargan-1@nasa.gov

Citation:
Wargan, K., Kramarova, N., Weir, B., Pawson, S., & Davis, S. M. (2020). Toward a reanalysis of stratospheric ozone for trend studies: Assimilation of the Aura microwave limb sounder and ozone mapping and profiler suite limb profiler data. *Journal of Geophysical Research: Atmospheres*, *125*, e2019JD031892. https://doi.org/10.1029/2019JD031892

Received 24 OCT 2019
Accepted 29 JAN 2020
Accepted article online 12 JUL 2019

Abstract Compatibility of the stratospheric ozone profile data from the Ozone Mapping and Profiler Suite Limb Profiler (OMPS-LP) and the Microwave Limb Sounder (MLS) is assessed in the context of a continuity requirement for future reanalyses. A methodology for the assimilation of OMPS-LP data into the Goddard Earth Observing System data assimilation system with a stratospheric chemistry module is developed. It is demonstrated that a simple homogenization technique significantly reduces the bias between OMPS-LP and MLS analyses. With the homogenization applied, the mean difference between the two analyses is within 3% and the difference standard deviation within 10%, consistent with the estimated uncertainties of the satellite ozone data. Larger differences are seen in the tropical lower stratosphere. The MLS and OMPS-LP assimilation experiments agree very well with independent data from ozonesondes and the Atmospheric Chemistry Experiment Fourier Transform Spectrometer. Heterogeneous ozone depletion during polar spring in both hemispheres as well as ozone transport during the 2016 quasi-biennial oscillation disruption event are realistically represented in both analyses. This work establishes a step toward achieving continuity of the post-2004 ozone record in future reanalyses, necessary for trend and long-term ozone variability studies, although further development is needed to address a drift in the OMPS-LP ozone data.

Plain Language Summary Following a period of decline in the second half of the twentieth century, stratospheric ozone has begun its road to recovery owing to the successful implementation of the Montreal Protocol and its amendments. Monitoring of the evolution of stratospheric ozone continues to be of interest to the scientific community and the public. This paper presents a step toward a future multidecadal analysis of stratospheric ozone using data from two types of satellite instruments: The Microwave Limb Sounder (MLS, 2004 to present) and the Ozone Mapping and Profiler Suite Limb Profiler (OMPS-LP, 2012 to present with projected future missions). We show that a simple homogenization methodology can be applied to remove the relative bias between the two data sets. We produce global records of stratospheric ozone for the year 2016 using a data assimilation methodology, which combines the satellite observations with an atmospheric chemistry model output. We show that MLS and OMPS-LP assimilation experiments are in excellent agreement with independent data and with each other, providing a strong basis for a consistent future multidecadal ozone reanalysis, in which OMPS-LP data will replace MLS once the latter becomes unavailable. We also emphasize that further work is needed to reduce a long-term spurious drift in OMPS-LP data.

1. Introduction

Stratospheric ozone is showing the first signs of recovery owing to the successful implementation of the Montreal Protocol of 1987 and subsequent amendments that phased out the production of ozone depleting substances (SPARC/IO3C/GAW, 2019; WMO, 2018). The future trajectory of ozone recovery and, in particular, the expected return date to the pre-1980 levels as well as the vertical distribution of the trends, exhibit

considerable sensitivity to the future concentrations of greenhouse gases via the dependence of chemical reaction rates on temperature and the dynamical responses of the stratospheric circulation to radiative forcing (Dhomse et al., 2018; Meul et al., 2016; WMO, 2018). Another source of uncertainty arises from unreported emissions of chlorofluorocarbons (Fang et al., 2019; Montzka et al., 2018) and effects of bromine-containing very short-lived substances (Oman et al., 2016). In addition, decadal-scale changes in stratospheric dynamics, whether forced or related to the internal variability of the climate system, have been shown to influence lower stratospheric ozone trends by partially counteracting its chemical recovery (Ball et al., 2018; Ball et al., 2019; Randel & Thompson, 2011; Wargan et al., 2018). These uncertainties merit the continuing monitoring of the evolution of stratospheric ozone through spatially resolved data sets in the context of the changing thermodynamics, dynamics, and chemistry of the atmosphere.

Atmospheric reanalyses provide multidecadal records of the atmospheric states at high spatial and temporal resolutions by merging multiple observational data sets through the data assimilation methodology, whereby the information from observations is propagated in space and time using general circulation models constrained by these observations. Error estimates of both observations and the model output are used to obtain an optimal estimate of the state of the atmosphere at every analysis time (typically, several times a day). Systematic differences among the diverse observations used in reanalyses during different periods pose a challenge for studies of long-term ozone variability and trends (Davis et al., 2017; Wargan et al., 2018). Several approaches to bias correction for multiple total ozone column observations were recently examined by Rochon et al., 2019, who used OMI as a reference. Wargan et al. (2018) developed a method of bias-correcting the ozone output from the Modern-Era Retrospective Analysis for Research and Applications, Version 2 (MERRA-2: Gelaro et al., 2017, Wargan et al., 2017) using a chemistry model simulation as a transfer standard to account for the discontinuity arising from the transition from nadir to limb-based ozone observing system in 2004. Based on that study, a future reanalysis using a single version of stratospheric ozone profile data should be adequate for detecting long-term ozone changes. MERRA-2 uses ozone profile observations from the Microwave Limb Sounder (MLS) on the Earth Observing System (EOS) Aura satellite from October 2004 onward. As MLS observations are expected to cease in the mid-2020s, the future stratospheric ozone reanalyses will utilize data from the Ozone Mapping and Profiler Suite Limb Profiler (OMPS-LP) instruments. The first OMPS-LP sensor was launched on the Suomi National Polar-orbiting Partnership satellite in 2011. This study is an assessment of the compatibility of the two observation types, which should extend the useful ozone reanalysis record into the next decades.

This study develops a methodology for assimilation of stratospheric ozone profiles from OMPS-LP, which involves a simple homogenization algorithm that significantly reduces the relative bias between OMPS-LP and MLS. We discuss the performance of MLS and OMPS-LP assimilation compared to independent data and previous studies, focusing on evaluation of the differences and similarities between assimilation experiments (*analyses*) that use MLS as the source of ozone profile information with those that utilize OMPS-LP. Ensuring a good agreement between MLS and OMPS-LP ozone analyses will be essential for the long-term ozone consistency in future reanalyses as the MLS record extends from late 2004 to present and the OMPS-LP instruments are projected to extend this record into the 2030s. Despite the need to use caution in interpreting trends computed from reanalyses (see Simmons et al., 2014), the post- 2004 ozone characteristics in MERRA-2 are well constrained by the MLS and OMI observations, to the extent that meaningful ozone trends can be computed (Wargan et al., 2018).

The year 2016 was selected for the test experiments since it featured several unusual events occurring in or affecting the stratosphere. Of particular interest are the following:

1. The boreal winter of 2015/2016 characterized by exceptionally cold and strong polar vortex and near-record ozone loss due to heterogeneous chemistry terminated by a relatively early final warming that began on 6 March 2016 (Khosrawi et al., 2017; Manney & Lawrence, 2016; Matthias et al., 2016).
2. The unusual disruption of the quasi-biennial oscillation (QBO; Osprey et al., 2016, Newman et al., 2016) that, combined with a very strong El Niño event, had a significant impact on tracer transport in the lower stratosphere (Diallo et al., 2018; Tweedy et al., 2017).

Section 2 describes the assimilated ozone data, independent observations, the data homogenization methodology, the data assimilation system, and experiments discussed in this study. Section 3 presents the results of comparisons of the OMPS-LP and MLS ozone data assimilation experiments with each other and with

independent observations and discusses the performance of the assimilated ozone with respect to springtime polar ozone loss and transport induced by the QBO disruption in 2016. A summary of our findings is given in section 4.

2. Methods

2.1. Assimilated Ozone Data

2.1.1. OMPS-LP

The OMPS-LP is one of the three OMPS instruments on the National Polar-orbiting Partnership satellite designed to provide long-term measurements for monitoring of stratospheric ozone. The OMPS-LP data are available starting March 2012 and continue to the present. Future OMPS-LP missions planned on the Joint Polar Satellite System 2, 3, and 4 are expected to deliver continued near-global ozone observations into the 2030s. Together with MLS, OMPS-LP will, therefore, provide an invaluable record of stratospheric ozone data spanning a period of about three decades during an especially important era of ozone recovery and climate change. The OMPS-LP design and long-term goals are described in Flynn et al. (2006). The sensor measures solar radiation in ultraviolet (UV) and visible (Vis) scattered from the atmospheric limb. Ozone is retrieved independently from UV (p < ~12 hPa) and Vis (~200–4 hPa) measurements. Retrievals from Vis and UV are treated as two independent data sources and are assimilated separately. The original National Aeronautics and Space Administration (NASA) retrieval algorithm for OMPS-LP was described by Rault and Loughman (2013). Version 2.5 of OMPS-LP ozone data used here was released in July 2017. Although the instrument is equipped with three slits, Version 2.5 of OMPS-LP data retrieve ozone profiles from only the central slit. OMPS-LP provides between about 2,200 and 2,500 UV and Vis profiles in the sunlit portion of the atmosphere per day. Extensive validation by Kramarova et al. (2018) found an agreement with independent satellite observations to within 10% between 18 and 42 km. Kramarova et al. (2018) also identified a positive drift in OMPS-LP of approximately 0.5% per year compared to MLS and the Odin Optical Spectrograph and InfraRed Imaging System observations. The retrieved ozone number densities on a constant 1-km altitude grid are converted to mixing ratio by volume using temperature data from the GEOS Forward Processing for Instrument Teams analysis, a product similar to MERRA-2. The mixing ratio at the same vertical grid is then assimilated as it is done for MLS.

We note that another OMPS-LP retrieved ozone product has been developed by Zawada et al. (2018). Unlike the one used here, it is based on a tomographic (two-dimensional) approach. Zawada et al. (2018) demonstrated the capability of the two-dimensional retrieval for resolving steep ozone gradients near the edge of the polar vortex when compared to an equivalent one-dimensional retrieval. We will discuss some implications of this in section 3.4.

2.1.2. MLS

The MLS instrument (Waters et al., 2006) onboard NASA's EOS Aura satellite (EOS Aura) measures microwave thermal emissions of the atmosphere. Its limb-viewing geometry allows retrievals of ozone mixing ratios at a vertical resolution of approximately 3.5 km in the stratosphere. As a microwave instrument, MLS provides measurements during both day and night. Unlike OMPS-LP, the MLS retrieval algorithm uses a two-dimensional approach, which accounts for inhomogeneities along the line of sight. We assimilate version 4.2 of MLS ozone (Livesey et al., 2018) between 215 and 0.1 hPa, as currently used in MERRA-2 (Wargan et al., 2018). Previous MLS ozone data versions have been evaluated by Froidevaux et al. (2008). As demonstrated by Hubert et al. (2016) MLS ozone data exhibit stability over the entire mission, from late 2004 to present, with no known drift. MLS generates approximately 3,500 profiles daily providing a near-global coverage during day and night between 82°S and 82°N. For completeness, we note that MERRA-2 assimilated version 2.2 of MLS ozone between 2004 and early 2015 and version 4.2 from that point onward. Starting May 2016 the 261-hPa level was dropped from assimilation in MERRA-2 leaving the 215-hPa level the lowest one assimilated as in this study.

2.1.3. OMI

The Ozone Monitoring Instrument (OMI; Levelt et al., 2018, 2006), also on EOS Aura, provides measurements of the total column ozone retrieved from backscattered solar ultraviolet radiation over the sunlit atmosphere. The assimilation experiments discussed below use OMI total ozone obtained from version 8.6 retrieval algorithm evaluated by McPeters et al. (2008). The treatment of OMI data in these experiments is identical to that in MERRA-2 (Wargan et al., 2017). Here, we note that the OMPS Nadir Mapper (NM)

Table 1
Locations and the Numbers of Soundings of the WOUDC and SHADOZ Ozonesondes Used in This Study.

Station name	Longitude	Latitude	Number of soundings
WOUDC			
Legionowo	20.96°E	52.41°N	27
Praha	14.44°E	50.00°N	51
Hohenpeissenberg	11°E	47.80°N	129
Payerne	6.57°E	46.49°N	146
Sapporo	141.33°E	43.06°N	47
Wallops Island	75.47°W	37.93°N	26
Tsukuba	140.13°E	36.06°N	47
Naha	127.69°E	26.21°N	44
Hong Kong Observatory	114.17°E	22.31°N	40
Maxaranguape (Natal)	35.26°W	5.49°S	30
Broadmeadows	144.95°E	37.69°S	46
Macquarie Island	158.94°E	54.50°S	48
Ushuaia	68.31°W	54.85°S	11
Marambio	56.62°W	64.23°S	28
Davis	77.97°E	68.58°S	22
Syowa	39.58°E	69.01°S	44
SHADOZ			
Pago Pago	170.71°W	14.33°S	33
Natal	35.26°W	5.49°S	42

sensors are expected to continue to provide total ozone data when OMI is no longer available. A preliminary analysis (not discussed here) demonstrates an overall good agreement between OMI and NM assimilation, although some differences are seen, particularly in the southern high-latitude assimilated total ozone (up to 10%) and in the troposphere. The assimilated stratospheric ozone is less affected as it is already well constrained by limb ozone data, although some impacts of a potential OMI-NP transition are expected there as well. Issues of continuity between OMI and NM-based total ozone assimilation are subject of ongoing research.

2.2. Validation Data

The primary source of independent validation data for lower- and middle-stratospheric ozone in this study are ozonesonde profiles from the World Ozone and Ultraviolet Radiation Data Centre database (WOUDC: WMO-GAW/WOUDC, 2017). Table 1 summarizes the ozonesonde locations and numbers of profiles. The majority of the WOUDC sondes are located outside of the tropics. Our analysis is supplemented with measurements from two tropical ozonesondes from Southern Hemisphere Additional Ozonesondes (SHADOZ) database. A recent reprocessing of these data removed artifacts due to varying operating procedures and changes in the instrumentation. Details of the reprocessing methodology are given in Witte et al. (2017, 2018) and Thompson et al. (2017). The two SHADOZ locations used are Pago Pago, American Samoa (170.71°W, 14.33°S, 33 profiles) and Natal, Brazil (35.26°W, 5.49°S, 42 profiles). Note that we use two versions of Natal data: from WOUDC and from SHADOZ.

Evaluation of assimilated stratospheric ozone is also done against the Atmospheric Chemistry Experiment Fourier Transform Spectrometer (ACE-FTS; Bernath et al., 2005). ACE-FTS provides solar occultation measurements, from which profiles of temperature, pressure, and concentrations of over 30 trace gases are retrieved. Version 3.5 ACE-FTS ozone was validated by Sheese et al. (2017) and found to be within 5% of observations by MLS and the Michelson Interferometer for Passive Atmospheric Sounding in the middle stratosphere and to exhibit a positive bias of 10% to 20% in the upper stratosphere and lower mesosphere. ACE-FTS is well-suited for evaluation of stratospheric ozone because of its high accuracy, high vertical resolution, and stability. These data were recently used by Errera et al. (2019) for a comprehensive evaluation of their chemical reanalysis of the stratosphere.

2.3. Data Assimilation System and Experiments

In data assimilation, information from (ozone) observations is combined with a background field from a short (6-hourly) model forecast, taking into account estimated uncertainties in the background and in the observations (Cohn, 1997). The resultant analysis state serves as an initial condition for the next assimilation time step. Analyses performed at NASA's Global Modeling and Assimilation Office (GMAO) use the Goddard Earth Observing System (GEOS) general circulation model (Molod et al., 2015) to provide the background states, and the Gridpoint Statistical Interpolation module to blend the background state with observations (Purser et al., 2003; Wu et al., 2002). The GEOS global circulation model together with the Gridpoint Statistical Interpolation module are referred to as the GEOS data assimilation system (GEOS-DAS).

The configuration of the system used in this study differs from that utilized in previous Global Modeling and Assimilation Office analyses (Wargan et al., 2015, 2017) in several important respects delineated below.

Rather than assimilating meteorological and radiance data that typically constrain the dynamics, the GEOS-DAS is run in a replay mode (Orbe et al., 2017). In this configuration the temperature and wind MERRA-2 fields are used to calculate forcing terms that constrain the GEOS general circulation model through the incremental analysis update methodology (Bloom et al., 1996), thus replicating the meteorological analyses and transport of chemical constituents from MERRA-2, in order to provide a controlled environment for the ozone assimilation. This configuration implicitly precludes feedbacks of the ozone assimilation on the

meteorological analyses, which would otherwise arise through the radiative forcing in the GEOS GCM and the use of infrared radiances in the meteorological assimilation.

GEOS ozone analyses, such as that in MERRA-2, have used a simple chemistry parameterization. The system used in our study employs a full stratospheric chemistry model, *StratChem*. This model, initially developed in the 1990s (Douglass et al., 1997; Kawa et al., 1995) has undergone substantial validation (Pawson et al., 2008) and further development (Nielsen et al., 2017). StratChem uses a family-based approach with 51 transported and 17 derived species. It includes a Nitric Acid Trihydrate polar stratospheric cloud scheme developed in Considine et al. (2000, 2003). In its present configuration, it simulates 125 thermal and 39 photolytic reactions, along with a representation of heterogeneous chemistry on polar stratospheric clouds. In particular, the scheme includes reactions involving very short-lived brominated species shown to be important for lower-stratospheric ozone, especially in the polar regions (Oman et al., 2016).

Two ozone assimilation experiments were performed with this system: (1) MLS analysis: assimilates ozone profiles from MLS; (2) OMPS-LP analysis: uses OMPS-LP data instead of MLS. In addition, both experiments assimilate total column ozone from OMI. Experiment (2) uses adjusted OMPS-LP data as described below. The experiments were run in a replay mode constrained by the MERRA-2 meteorological fields for the 13-month period from December 2015 to December 2016.

2.4. Modeling of Observation Error and Quality Control

The OMPS-LP ozone retrievals include a measure of precision. Experimentation showed that using these estimates as observation errors led to a weak fit to the data in the assimilation system. The results presented here use an observation error in which the provided precision estimate is multiplied by a factor of 0.75, which produces a better agreement with independent data. We note that the reported precisions in version 2.5 OMPS-LP retrievals (Kramarova et al., 2018) are larger than those in the previous versions and are likely to be overestimated. It is common in data assimilation to tune the observation errors to best fit the assimilated as well as independent data. Strict data screening was used for quality: The only retrievals used had quality flag set to 1 and a "SwathLevelQualityFlags" of zero (see DeLand et al., 2017). In particular, this excluded OMPS-LP observations affected by the South Atlantic Anomaly, the Moon, solar eclipses, or other planets in the field of view. In addition, in the layer where UV and Vis overlap (approximately between 12 and 4 hPa) all data for which the difference between the UV and Vis retrievals exceeded the reported precision were excluded. Overall, this amounts to about 50% of all observations being rejected, more in the northern high latitudes than elsewhere. This highly selective quality control of the OMPS-LP data does lead to a substantial reduction in number of profiles assimilated, but the results discussed below indicate that the remaining data are sufficient to constrain the analysis ozone in the middle stratosphere. It is possible that some of these criteria can be relaxed in the future, as the data and their possible errors become better understood.

2.5. Adjustment of OMPS-LP Ozone Data

Figures 1a and 1b show the zonal mean difference between OMPS-LP ozone and MLS observations of the sunlit atmosphere averaged over the period 2013–2017 for the UV and Vis products separately as a function of latitude (in 5° bins) and pressure. The bias is calculated on a monthly basis within a given latitude bin and if there are at least 200 MLS and OMPS-LP observations in that bin and month. The Vis bias is mostly negative (Vis ozone is lower than MLS) with the exception of positive values in the tropical middle stratosphere, a layer between 80 and 20 hPa in the tropics and northern middle latitudes, and a region of small positive values between 70°S and 60°S, 50 to 10 hPa. This layered structure appears to "bend" upward with latitudes decreasing toward the South Pole. The bias in UV is mainly positive between 8 and ~2 hPa and negative above. The spatial structure of the bias is different between UV and Vis, providing a strong argument for treating these two retrievals as separate data sources in assimilation. The relative bias is larger in the upper troposphere-lower stratosphere (UTLS) where ozone mixing ratios are smaller. These differences between the OMPS-LP and MLS ozone retrievals are consistent with those in Kramarova et al. (2018) (their Figures 8 and 9).

The following adjustment procedure was applied to the OMPS-LP data. It was performed separately for the Vis and UV data. The zonal mean OMPS-LP minus MLS differences were calculated on the MLS pressure levels for each month, then averaged between 2013 and 2017. The MLS measurements of only the sunlit

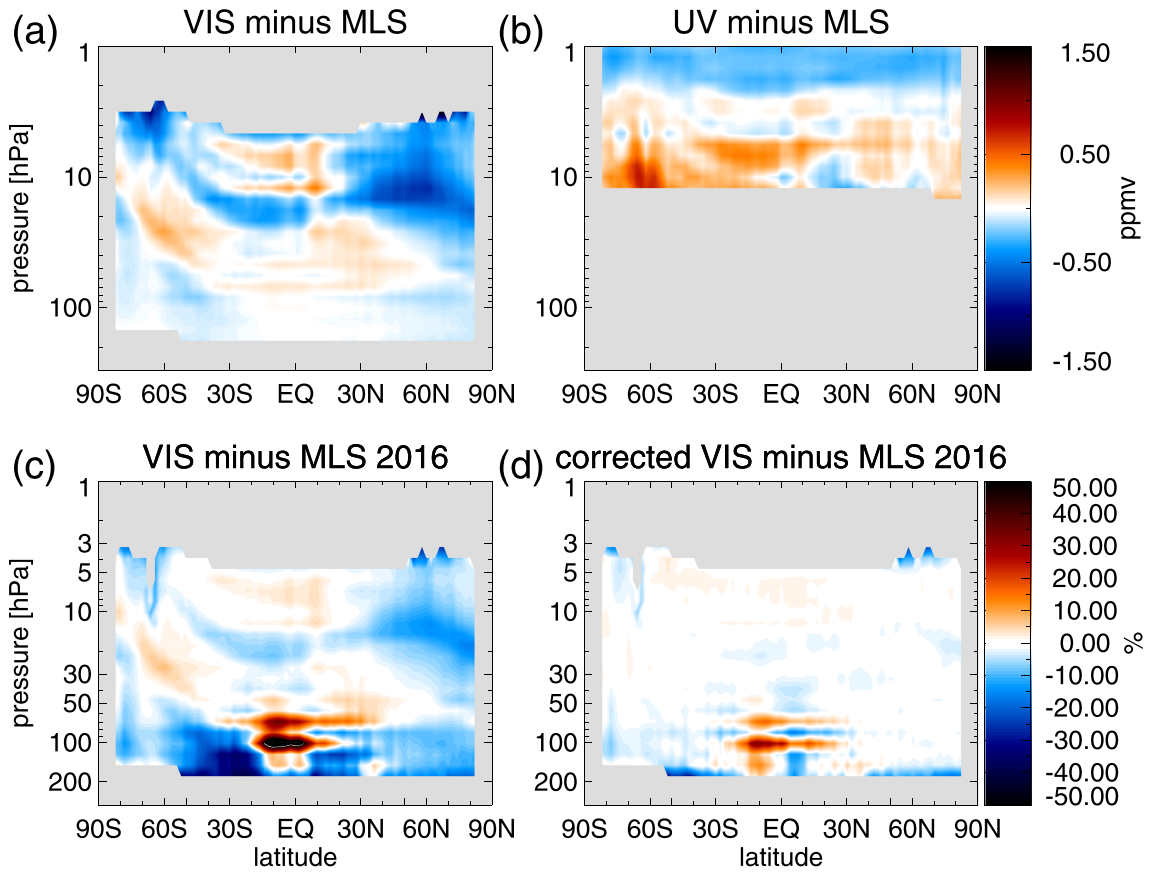

Figure 1. (top row) zonal mean OMPS-LP bias with respect to MLS averaged 2013–2017 and shown in parts per million by volume. (a) Visible retrievals; (b) UV retrievals. (bottom row) 2016 averaged Vis minus MLS difference relative to the MLS mean (c); 2016 averaged difference between adjusted Vis and MLS relative to MLS mean. Regions with no data are shown in gray. In (c) and (d), the white areas represent differences within 1%.

portion of the atmosphere were used. This produced 12 lookup tables containing biases as functions of latitude and pressure. These biases were then interpolated to the OMPS-LP observation locations and subtracted from every OMPS-LP profile. The normalization of the OMPS-LP ozone data sets to MLS does not imply an assumption that the latter are more correct than OMPS-LP. Rather, the purpose of this procedure was to eliminate discontinuities that would otherwise arise when merging the two data records by assimilation. The adjustment procedure described above does not guarantee that there will be no mean difference between MLS and OMPS-LP at any given month, year or location; it simply removes the zonal, temporal (2013–2017) mean difference, thus significantly reducing the discontinuity between the two data sets.

The substantial impacts of applying this adjustment to OMPS-LP Vis in 2016 are evident by contrasting the original differences (Figure 1c) with the adjusted values (Figure 1d). In much of the stratosphere the differences between adjusted OMPS-LP and MLS are within 1%. As an example, at pressures greater than 70 hPa, the extratropical ozone is 20–40% lower in OMPS-LP than in MLS, and the adjustment reduces this difference to less than 10% except at the lowest extent of the retrievals. In the Tropics, Figure 1c shows an alternating pattern of negative and positive differences, consistent with spurious oscillations in the lower-stratospheric MLS ozone, which are smaller in Version 4.2 than prior versions (Livesey et al., 2018); these are reduced in magnitude, but not completely eliminated, by the adjustment (Figure 1d). There are two reasons for this: first, the alternating positive and negative OMPS-LP/MLS differences change from year to year; second, the limited vertical resolution of both data sets, combined with their different vertical grids, means there is not enough information in the mean profiles to completely suppress these oscillations.

While in most of the stratosphere the relative bias between the two satellite data sets is small compared to climatological ozone mixing ratios, there are regions where it is significant and could introduce spurious

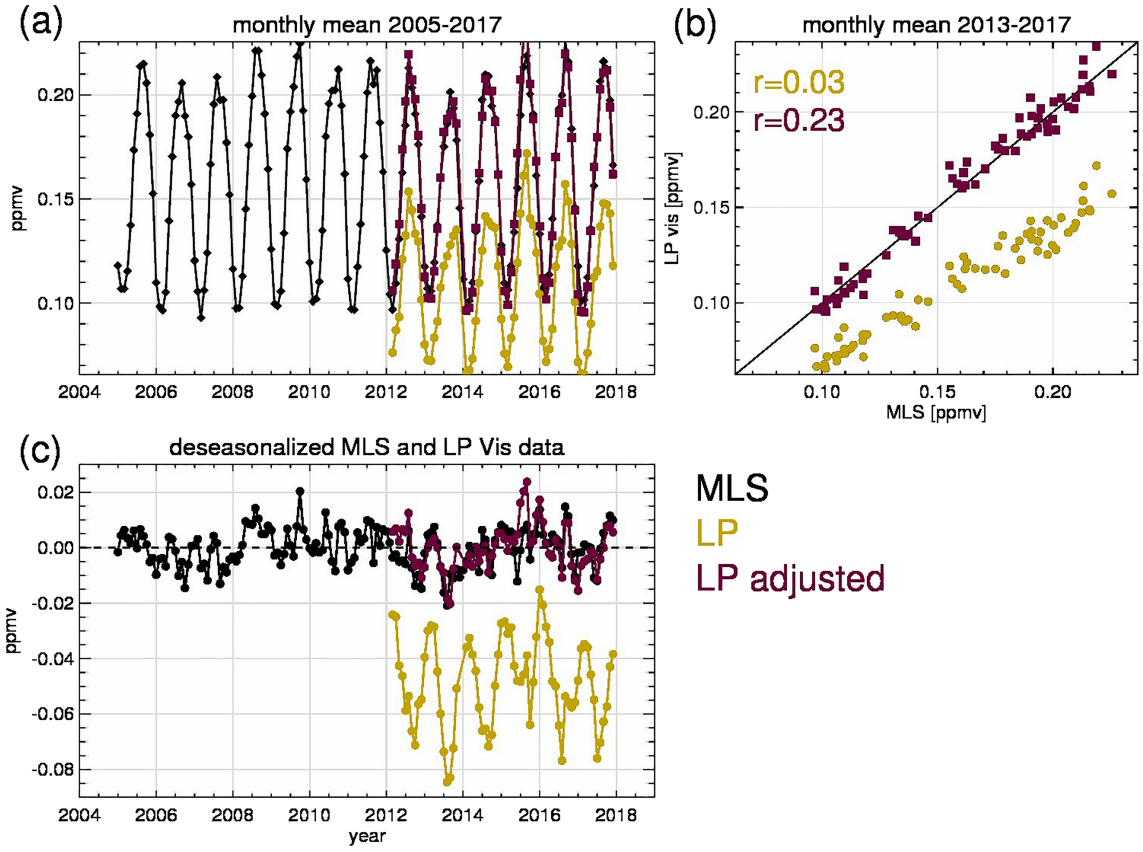

Figure 2. (a) Time series of monthly MLS ozone at 150 hPa averaged between 40°S and 30°S (black). The corresponding OMPS-LP (Vis) time series before and after adjustment are shown in yellow and magenta, respectively. (b) Scatterplot of OMPS-LP unadjusted and adjusted data as in panel (a). (c) Deseasonalized MLS data (black), deseasonalized OMPS-LP data (magenta) and the latter minus the monthly adjustment (yellow).

discontinuities in the assimilated ozone if OMPS-LP were to replace MLS or if the two data sets were to be assimilated jointly. Figure 2 illustrates a particularly severe case. At 150 hPa between 40°S and 30°S OMPS-LP Vis ozone is lower than MLS by about 30% (Figures 2a and 2b). In addition, the seasonal amplitude of OMPS-LP ozone is less than that of MLS (Figure 2a), indicating a seasonal dependence of the bias. The results of the OMPS-LP adjustment are illustrated in Figures 2a and 2b in magenta. The adjusted OMPS-LP data overlap with MLS and the already high correlation between the two data sets improves slightly from 0.97 to 0.99. Figure 2c shows the deseasonalized MLS and OMPS-LP anomalies obtained by removing the monthly climatology calculated from each data set separately. Here again, an overall good agreement is evident despite some small differences in 2012 and 2015. Also shown is a time series of OMPS-LP anomalies offset by the monthly OMPS-LP minus MLS differences (the yellow line). It is clear that the offset in this region as well as the differences in the seasonal amplitudes between the two data sets are quite large compared to interannual variability. If assimilated without homogenization these differences would pose a serious problem for studies of long-term variability and trends.

3. Results

3.1. Overall Performance of the Experiments

The fit of MLS and (adjusted) OMPS-LP analyses to the observations assimilated by each experiment is examined. For each observed ozone value, the GEOS-DAS outputs an observation minus background (O-B) residual, which measures the discrepancy between that observation and the model-generated ozone state interpolated to the observation location before assimilation. Analogously, an observation minus analysis (O-A) residual is the difference between that observation and the analysis ozone after the current assimilation step. It is expected that O-As are closer to zero than O-Bs on average. Figure 3 shows the

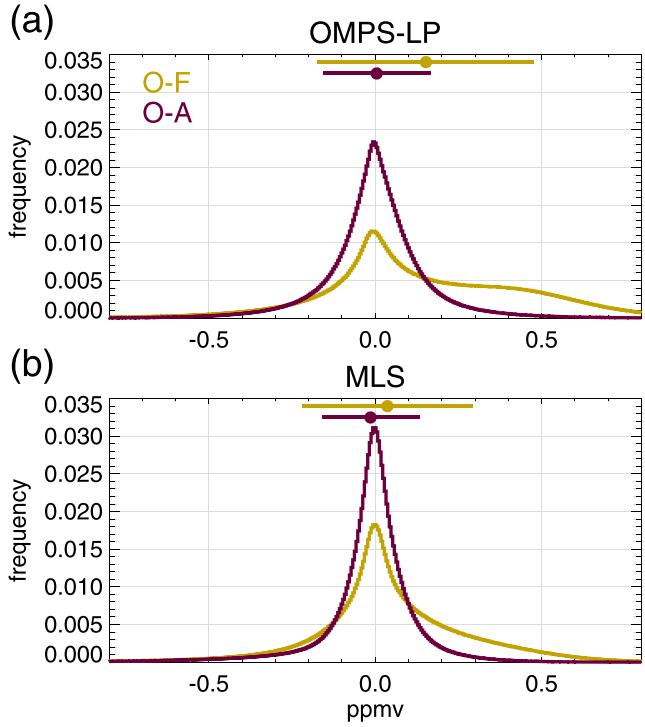

Figure 3. Probability density functions (PDFs) of global observation minus background (O-B, yellow) and observation minus analysis (O-A, magenta) differences for (adjusted) OMPS-LP (a) and MLS (b). All 0 and 12 UTC data in 2016 are used. The horizontal lines near the top of each panel show the mean (filled circles) ±1 standard deviation of each PDF.

probability density functions (PDFs) of the O-Bs and O-As for OMPS-LP and MLS calculated for the entire year 2016 (two 6-hourly time windows per day are used: 21–3 UTC and 9–15 UTC). For both experiments the mode and the mean of the O-B PDFs are already close to zero and further reduced in the O-As. The O-As are a factor of 1.75 smaller than the O-Bs for MLS and 2.01 smaller for OMPS-LP. For both data sets the O-B PDFs are fat-tailed toward larger positive values. This is especially evident in the OMPS-LP O-Bs where the relatively large frequencies between 0.1 and 0.8 ppmv result from a large number of high UV ozone values close to the peak of the mixing ratio around 10 hPa in the tropics. We note that the adjustment applied to OMPS-LP only shifts the data distribution mean leaving the higher moments unaffected. The skewness is greatly reduced by assimilation. These results provide a measure of the impact that assimilated ozone profile observations have on an analysis but they cannot be used to assess the quality of the assimilated product. The latter is accomplished through comparisons with independent (nonassimilated) data presented in sections 3.2 and 3.3.

Figure 4 shows the 2016 zonal mean difference and difference standard deviation between the MLS and OMPS-LP analyses, expressed relative to the MLS experiment. Also shown is the zonal mean 2016 ozone mixing ratio from the MLS experiment. The 0.1 ppmv MLS contour can be taken to approximate the tropopause. As expected, at pressures between 200 and 10 hPa the differences between the two analyses exhibit a similar structure to those between adjusted OMPS-LP Vis and MLS (Figure 1d). In most of the stratosphere the differences are close to zero, except in the tropics where some of the oscillating pattern discussed above is evident, although weaker than in Figure 1d, reflecting a mitigating impact of the model dynamics and chemistry on the assimilation. In the upper stratosphere (constrained by UV in the OMPS-LP experiment) the largest differences are within 3–4%. As there are almost no OMPS-LP observations to constrain the analysis at pressures higher than 200 hPa, the differences between the two analyses are much larger there, reaching up to about 40%.

The agreement between the two experiments in terms of their difference standard deviations is very close, indicative of a similar temporal ozone variability driven, in both cases, by the same MERRA-2 meteorology. The difference standard deviations are less than 10% (relative to the MLS analysis average) in most of the stratosphere and within 3% between 60°S and 60°N at pressures less than 50 hPa. Larger standard deviations are seen in the tropical UTLS (at pressures greater than 50 hPa) and around the extratropical tropopause where OMPS-LP observations are not assimilated.

In the lower stratosphere the differences exhibit some longitudinal structure. Figure 5a shows the difference between the OMPS-LP and MLS analyses at 100 hPa averaged between March and May 2016 and expressed as a percentage of the average ozone from the MLS experiment. The differences maximize over the central Pacific between the equator and 30°S where the OMPS-LP experiment produces values up to 28% higher than the MLS analysis. Standard deviations of the differences between the two analyses at 100 hPa are shown in Figure 5b. The maximum difference standard deviations are seen, again, in the tropical Pacific. They reach up to 36% in the same region where the mean difference attains a maximum. Outside of the tropics the difference standard deviations are within 20%, typically less. Ozone retrievals from OMPS-LP in the upper troposphere and lower stratosphere can be affected by aerosols, water vapor, and clouds. While the retrieval algorithm attempts to remove the observations affected by clouds (Chen et al., 2016) some thin clouds may go undetected. Furthermore, clouds can still affect the retrieval even if they are not directly at the instrumental line of sight. An analysis of Vis and MLS observations at 100 hPa in the first months of each year between 2014 and 2017 (not shown) reveals that the maximum positive differences are located over the maritime continent in the non-El Niño years and shifted toward the Central Pacific in 2016 raising a possibility that these differences are related to deep convection. Furthermore, at the beginning of 2016 OMPS-LP measurements indicated elevated aerosol amounts over this region, which could contaminate the ozone

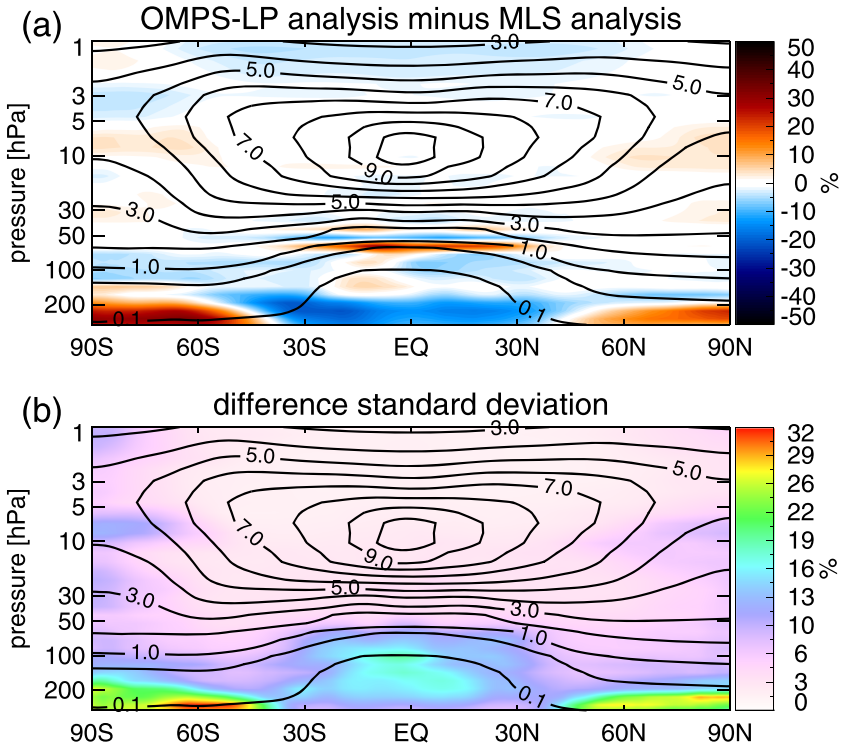

Figure 4. Zonally averaged difference between the MLS analysis and the OMPS-LP analysis ozone calculated for 2016 and expressed as percentage of the MLS analysis mean (a). Difference standard deviation between the two experiments in 2016 relative to the MLS analysis (b).

signals: this issue is currently being investigated. Outside of that region the discrepancy between the experiments is much smaller and mainly negative.

3.2. Lower and Middle Stratosphere: Comparisons With Ozonesondes

In this section, the performance of the MLS and OMPS-LP analyses in the lower and middle stratosphere is evaluated using the independent data from WOUDC ozonesondes. The results are presented in the form of joint PDFs (ozonesonde-analysis) using all available data from 2016. In addition, the first and second moment statistics and ozonesonde-analysis correlations were computed. The comparisons were done as follows. First, both analyses were interpolated in the horizontal to ozonesonde locations and times, then all data were mapped onto the tropopause-relative vertical grid. Here, the tropopause was defined as the 2-PVU (potential vorticity unit) surface or the 380-K isentrope, whichever was located at a lower altitude. The use of the tropopause-relative vertical coordinate amounts to the removal of the portion of the tracer variability that arises solely from local, geographical and climatological variations in the tropopause height. Similar approach was used, for example, by Sofieva et al. (2014) to construct an ozone climatology from ozonesondes and satellite data, and by Wargan et al. (2015, 2017) to separate tropospheric and stratospheric air masses for evaluation of assimilated ozone.

Figure 6 shows the joint PDFs of the ozonesonde and analysis ozone at six levels: 0, 1, 3, 5, 10, and 15 km above the tropopause. About 700 ozonesonde soundings were used. Overall, the agreement between the assimilation experiments and ozonesondes improves with the distance from the tropopause. At the lowest two levels the difference standard deviations are within 0.06 ppmv. Specifically, at the tropopause the standard deviations are up to 39% of the sonde mean of 0.1 ppmv for both MLS and OMPS-LP analyses. At 1 km above, the standard deviations are 27% and 30% of 0.2 ppmv for MLS and OMPS-LP, respectively. The average sonde - analysis difference is up to 0.01 ppmv at the tropopause and at 1 km above (2–3%). Importantly for this study, the PDFs are very similar between the two experiments, with the OMPS-LP analysis showing only slightly worse agreement with the sondes in terms of the scatter and correlation coefficient. The

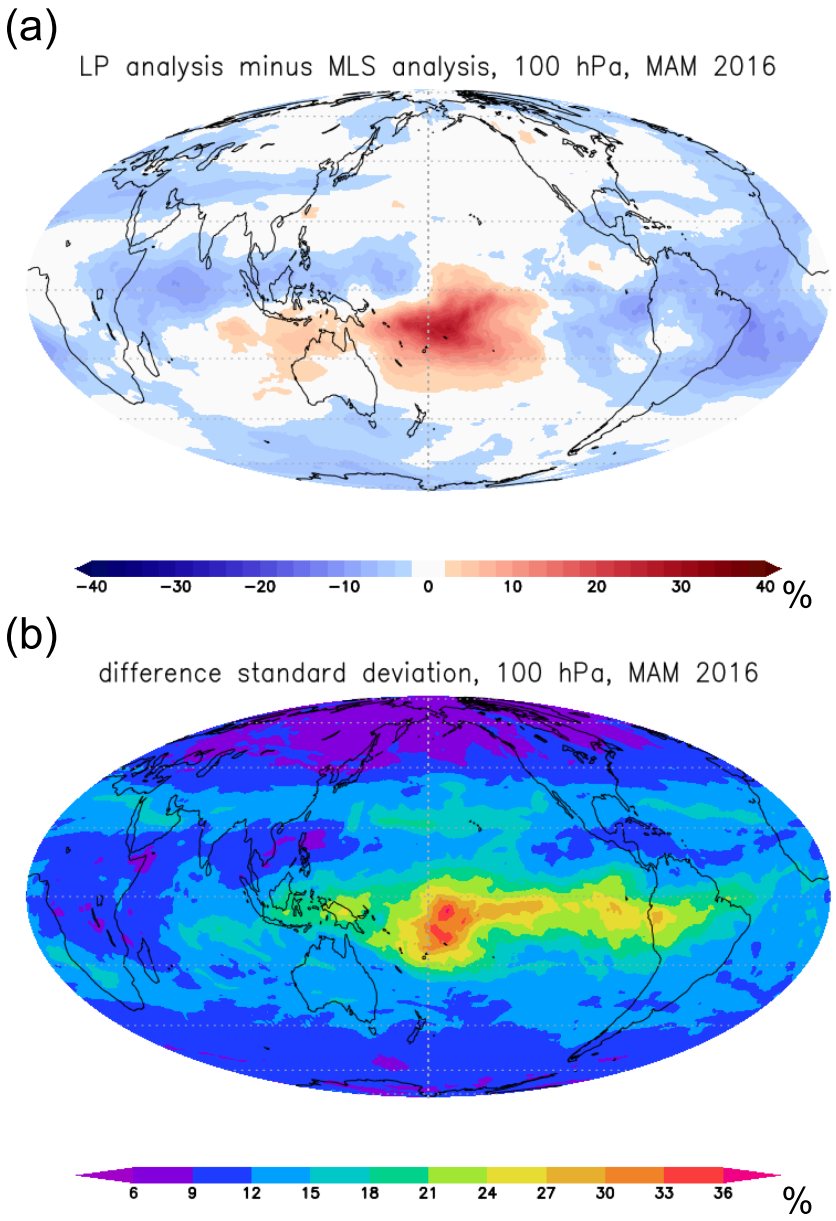

Figure 5. Percent difference (a) and difference standard deviation (b) between ozone from the OMPS-LP and MLS experiments at 100 hPa calculated over the period from march to may 2016 and shown relative to the MLS analysis.

analysis-ozonesonde correlations at the tropopause are 0.74 and 0.71 for the MLS and OMPS-LP analyses, respectively. At 3 km, the agreement between both experiments and ozonesondes is very good, with a bias within 3%, difference standard deviations of 23% for both experiments, and correlations above 0.9. Again, the PDFs and the statistics are very similar between the two analyses. At 5, 10, and 15 km above the tropopause both experiments exhibit an excellent agreement with the ozonesondes. The average differences do not exceed 0.07 ppmv and the difference standard deviations are all within 0.4 ppmv. All the analysis-ozonesonde correlations at these levels are close to unity. These high correlations indicate a strong covariability, part of which arises from climatological latitudinal and seasonal patterns being well captured by the analyses. In order to test the ability of the assimilation to reproduce also short-term dynamically driven variability we repeated these calculations for ozonesondes within 40–60°N and 10°W to 25°E and during a single season, March to May. There were 107 ozonesondes matching these criteria. In this case the correlations at the selected levels from the tropopause up are 0.35, 0.8, 0.87, 0.88, 0.97, and 0.96 for the MLS analysis and 0.42, 0.82, 0.87, 0.91, 0.97, and 0.95 for the OMPS-LP experiment,

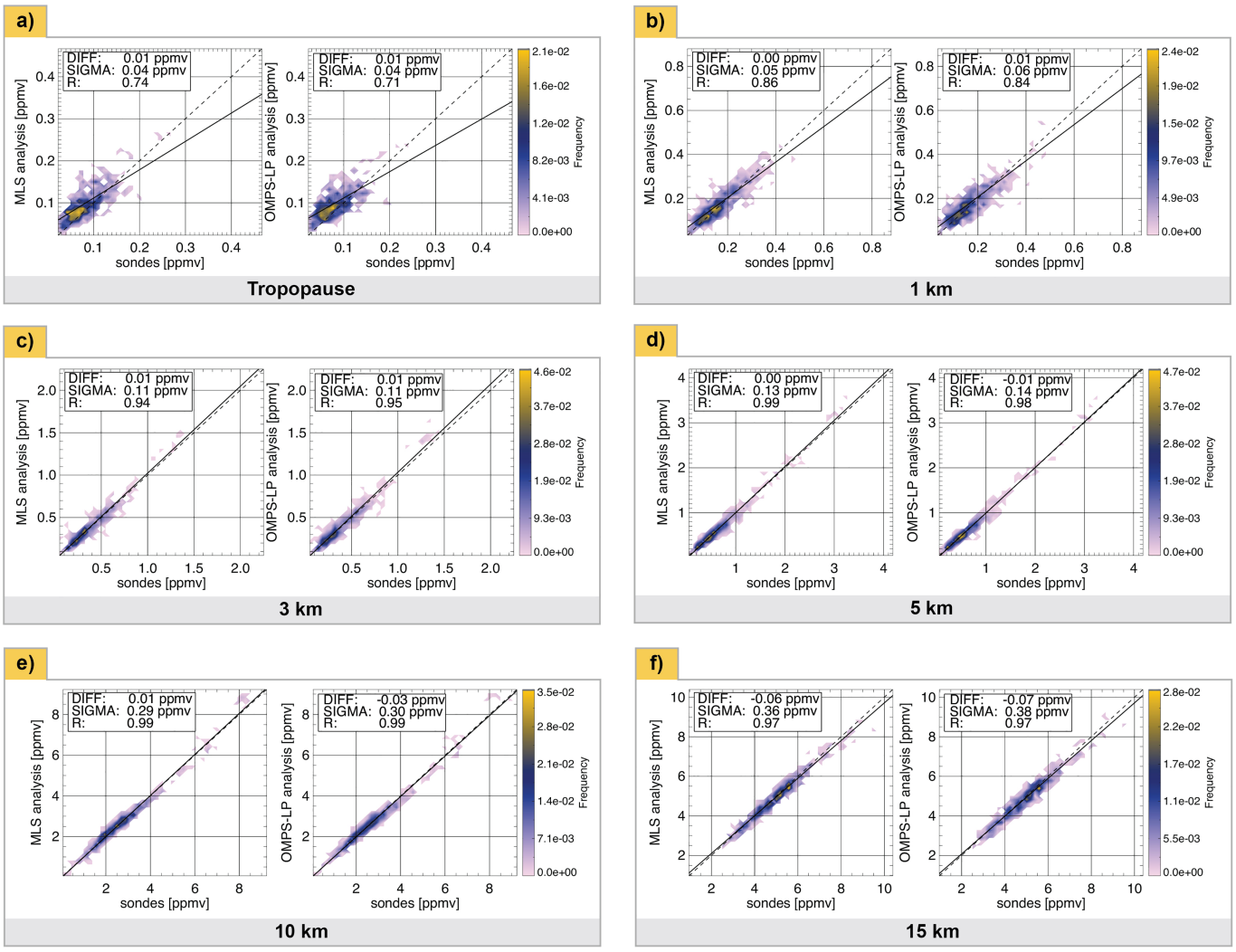

Figure 6. Joint probability distribution functions of ozone (ppmv) from ozonesondes and MLS analysis (left panels) and ozonesondes and OMPS-LP analysis (right panels) at the tropopause (a) and selected levels above the tropopause: 1 km (b), 3 km (c), 5 km (d), 10 km (e), and 15 km (f). The dashed and solid lines are diagonals and linear fits to the data, respectively. Mean differences (analysis minus sondes), standard deviations of the differences, and ozonesonde-analysis correlations are given in inset boxes. Note that the color scales differ among the plots.

indicating an excellent ability of both analyses to represent the dynamical and chemical variability of ozone throughout the lower and middle stratosphere.

We will now examine the differences between the OMPS-LP and MLS experiments in the tropical lower stratosphere over the Central Pacific and the west Atlantic where the differences are particularly large (Figure 5). Daily time series of ozone mixing ratio at two tropical locations: Pago Pago, American Samoa (170.71°W, 14.33°S), and Natal, Brazil (35.21°W, 5.84°S) at 100 and 70 hPa are shown in Figure 7 along with available observations from the SHADOZ ozonesondes. Overall, the analyses follow each other closely. At Natal there is a pronounced seasonal cycle at 70 hPa with a minimum in May and maximum around October. At 100 hPa at the same location there are two maxima: one in January and one in July. At Pago Pago in June, a sudden increase in ozone mixing ratios is evident at 70 hPa and a slower increase is seen at 100 hPa. All those characteristics are seen in both analyses and are supported by the ozonesonde observations. The largest discrepancies between the analyses are seen at Pago Pago at 100 hPa between January and April (corresponding to the maximum difference seen in Figure 5) and at Natal at 70 hPa between June and August. In both cases the OMPS-LP analysis produces higher values. At Pago Pago the ozonesondes agree with MLS better, while at Natal at 70 hPa it is OMPS-LP that is in a closer agreement with the sondes.

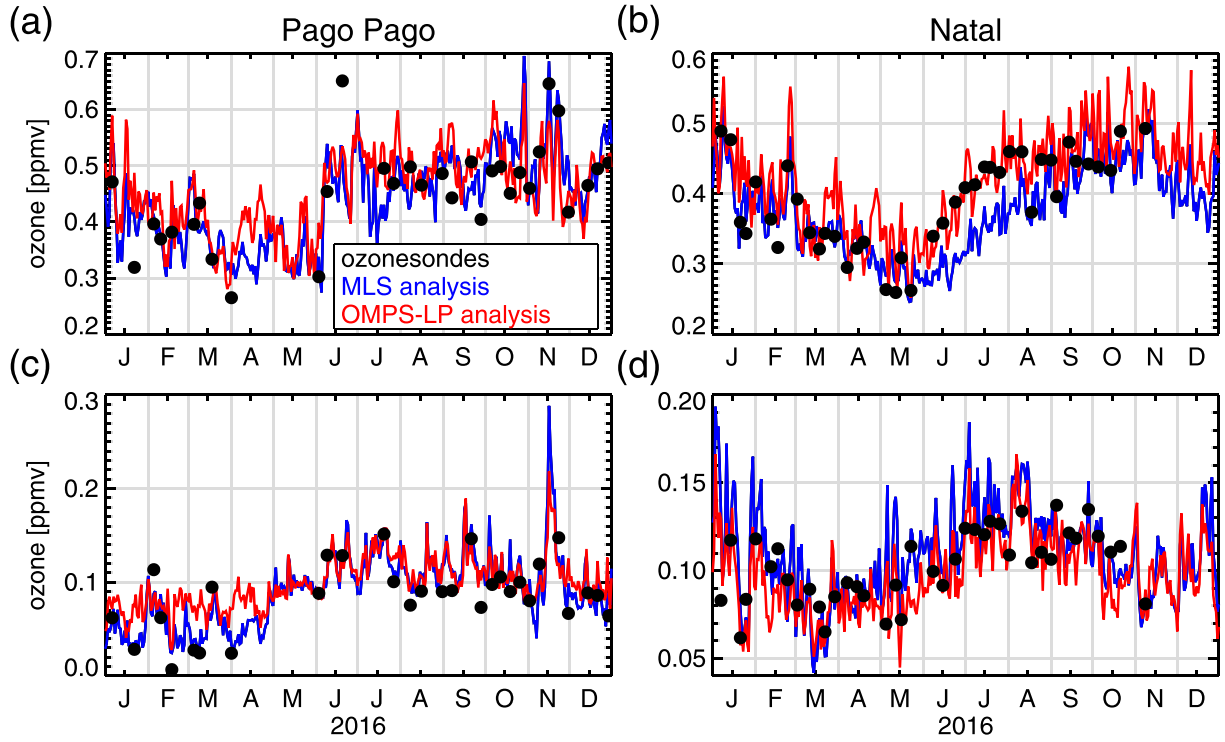

Figure 7. Time series of daily ozone at Pago Pago (a and c, 170.71°W, 14.33°S) and Natal (b and d, 35.26°W, 5.49°S) at 70 hPa (a and b) and 100 hPa (c and d) from the MLS analysis (blue), OMPS-LP analysis (red), and SHADOZ sondes (black circles).

The above analysis is meant to illustrate the differences between the two experiments where they are the largest: in the tropical lower stratosphere. Overall, the performance of the OMPS-LP and MLS analyses is very similar.

3.3. Middle and Upper Stratosphere: Comparisons With ACE-FTS

Figure 8 shows joint probability distribution functions of ACE-FTS ozone and the two experiments at six selected model levels between 50 and 1 hPa. All available quality-screened ACE-FTS data from 2016 were used (6,229 profiles). The coverage of the instrument varies from month to month with a maximum number of observations at midlatitudes and no observations north of about 80°N and south of 80°S.

The absolute values of the ACE-FTS analysis differences and standard deviations are given in Figure 8. Below we report the same statistics relative to the ACE-FTS averages at each level. At 43.9, 26.05, and 8.46 hPa the differences between the experiments and ACE-FTS range between 2.1% and 4.2% for the MLS analysis and between 1.6% and 2% for the OMPS-LP experiment. The difference standard deviations are within 8% for both experiments. At 4.56 and 1.95 hPa the relative differences are within 3% for both experiments and the difference standard deviations do not exceed 6%. Higher differences are seen at the stratopause: At 0.91 hPa both analyses are lower than ACE-FTS by 0.22 ppmv (MLS) and 0.39 ppmv (OMPS-LP) or 9.6% and 11.6%, respectively. This is consistent with the 10–20% high bias of ACE-FTS ozone with respect to other satellite data sets found by Sheese et al. (2017). We note that, due to very short chemical time scales for ozone in the upper stratosphere, the effects of data assimilation are quickly removed and the analysis ozone near the stratopause is largely driven by the model chemistry

Both analyses exhibit very high correlations with ACE-FTS. The PDFs maximize along the diagonals with almost no indication of significant outliers. One exception is a number of high ozone concentrations produced by the OMPS-LP analysis at 8.46 hPa and corresponding to about 4 ppmv in ACE-FTS data. We have determined that these high values result from an overestimation of ozone by the analysis at high latitudes in May as the polar night stratosphere is not observed by OMPS-LP.

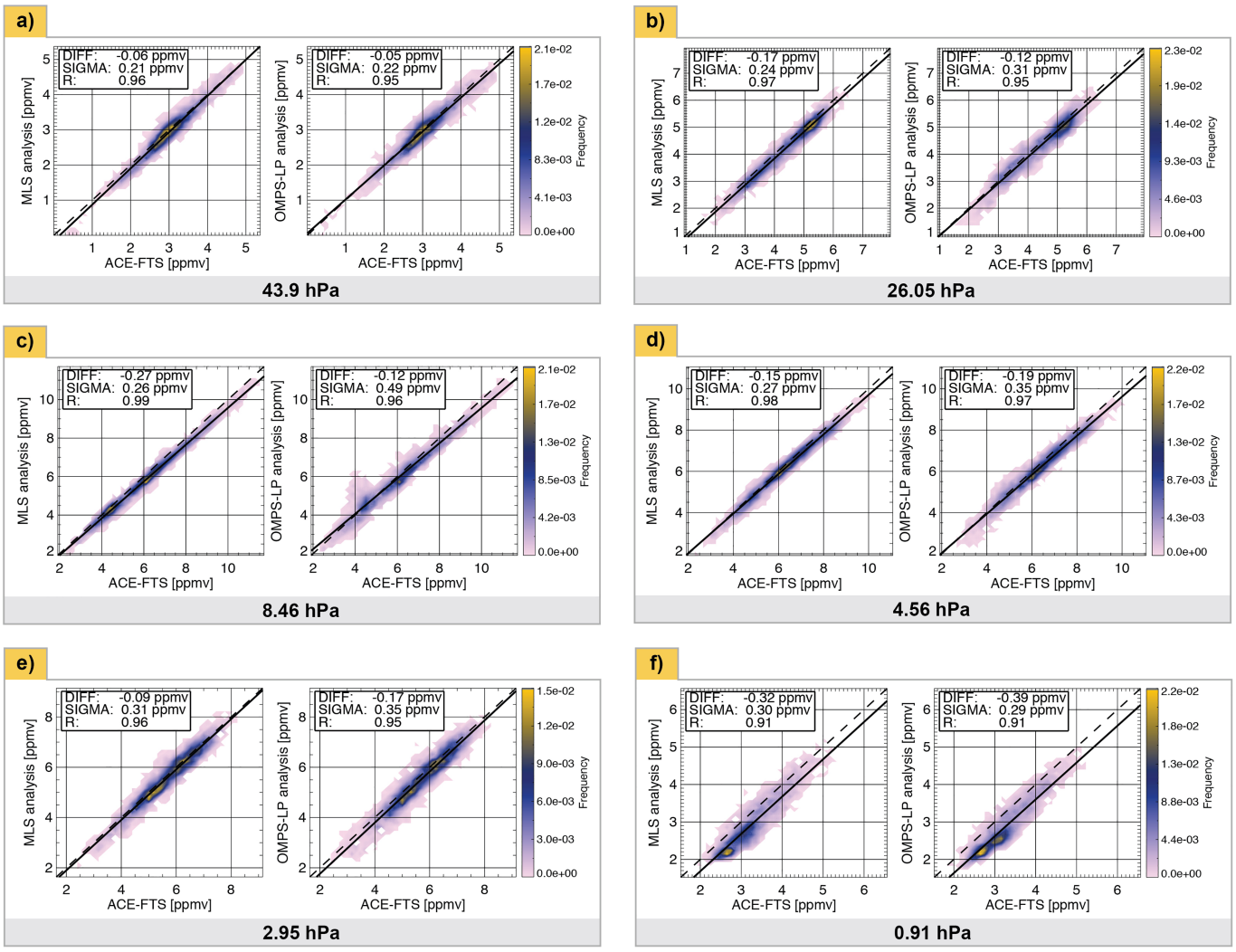

Figure 8. Joint probability distribution functions of ozone (ppmv) from ACE-FTS and MLS analysis (left panels), and ACE-FTS and OMPS-LP analysis (right panels) at selected GEOS model levels: 43.9 (a), 26.05 (b), 8.46 (c), 4.56 (d), 2.95 (e), and 0.91 hPa (f). The dashed and solid lines are diagonals and linear fits to the data, respectively. Mean differences (analysis minus ACE-FTS), standard deviations of the differences and ozonesonde-analysis correlations are given in inset boxes. Note that the color scales differ slightly among the plots.

3.4. Process-Based Evaluation

3.4.1. Arctic Winter Ozone Depletion

Manney and Lawrence (2016) demonstrated that the maximum ozone loss due to heterogeneous chemistry during the 2015/2016 polar winter occurred near the 490-K potential temperature surface. Here, we discuss the analysis results on a nearby 480-K isentrope (about 20 km above the surface). Figure 9 shows maps of ozone from the MLS (a) and OMPS-LP (b) analyses separately on the 480-K isentrope at 12 UTC on 15 December 2015, 15 January 2016, 15 February 2016, and 15 March 2016. Differences between the two analyses are shown in Figure 9c. The polar vortex edge is defined as the location of the maximum gradient of the isentropic potential vorticity as in Nash et al. (1996), with an additional smoothing of the vortex edge PV values by a 15-day Fourier low-pass filter.

On 15 December the maximum ozone mixing ratios, reaching over 3.25 ppmv, are found inside the vortex with patches of lower values seen over Siberia. At midlatitudes ozone is 2 ppmv and lower at most locations. In mid-January the polar vortex is elongated and stretched between eastern Canada and northern Europe. The concentrations within the vortex are still high and ozone begins to form a collar around the vortex edge. The collar is fully formed by 15 February while the mixing ratios inside the vortex are now much lower,

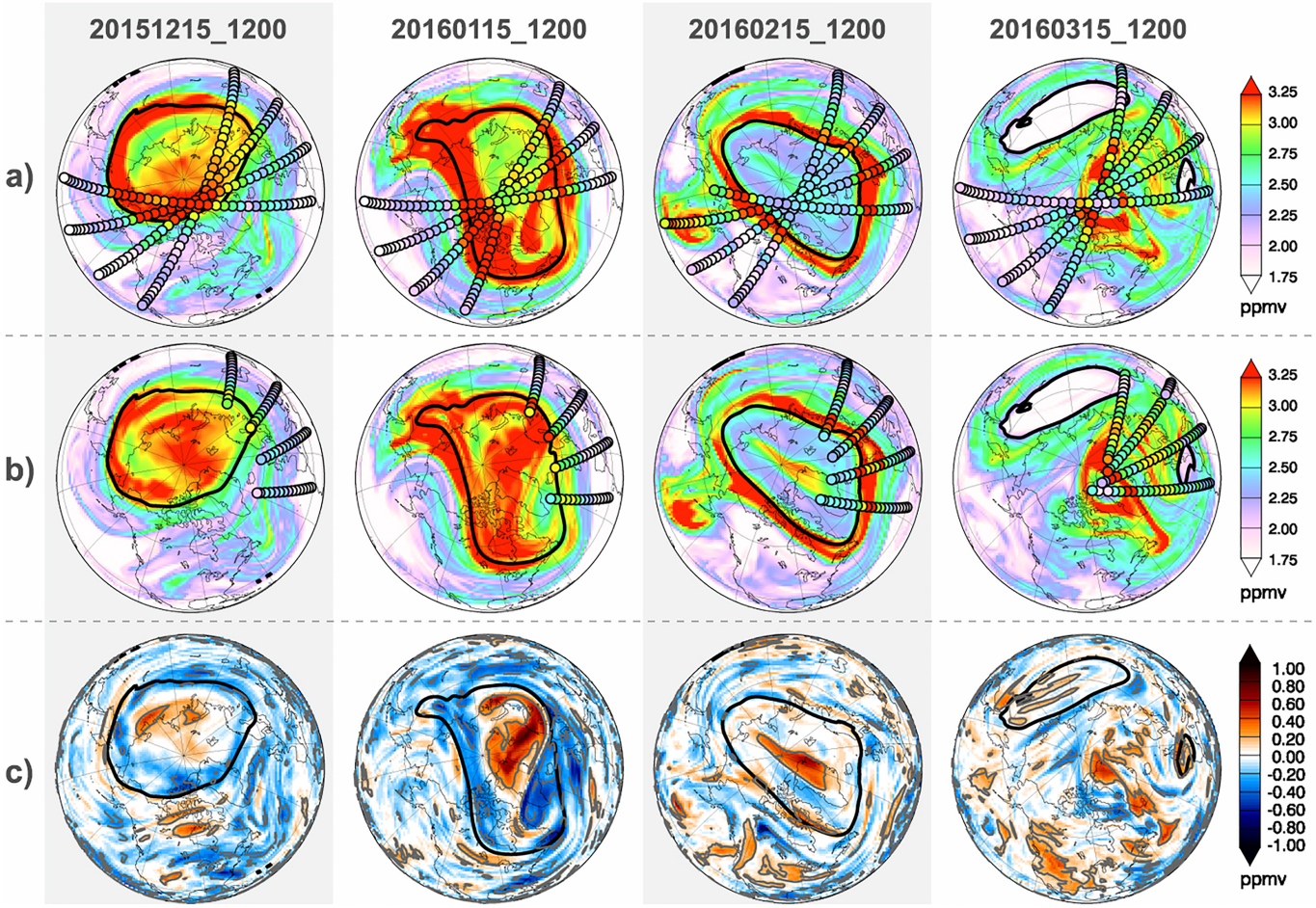

Figure 9. (a) Maps of ozone in ppmv at the 480-K isentrope from the MLS analysis at 12 UTC on (from left to right) 15 December 2015, 15 January 2016, 15 February 2015, and 15 march 2015. (b) the same for the OMPS-LP analysis. The circles show locations and values of the assimilated ozone observations from (a) MLS and (b) OMPS-LP, taken between 9 and 15 UTC on each day shown. In the interest of clarity only every other data point is shown but the northernmost observation locations from OMPS-LP are included. (c) Differences between the MLS and OMPS-LP analyses relative to the MLS analysis. The −10% and 10% contours are shown in gray, solid, and dashed, respectively. The thick black contours in all the plots indicate the edge of the polar vortex.

between 2.25 and 2.75 ppmv, indicative of rapid chemical depletion (Khosrawi et al., 2017). We note that the presence of a patch of higher values deep inside the vortex surrounded by lower ozone closer to the edge, evident in Figures 9a and 9b on 15 February, is consistent with the depletion occurring in the sunlit region of the vortex where ClOOCl molecules are photolyzed to ClOO and atomic chlorine that subsequently catalyzes ozone destruction. As a result of a final warming that began on 5–6 March the polar vortex became displaced off the pole and split into three offspring vortices (Manney & Lawrence, 2016). This is seen in Figures 9a and 9b on 15 March: One large vortex fragment is located over Siberia and a smaller one travels westward south of Great Britain. The third fragment (without a well-defined edge) is seen over the north-western Greenland. Ozone is largely depleted within the offspring vortices with mixing ratios of 1.75 ppmv and lower in the largest fragment. The morphology of the ozone fields is very similar between the two analyses. This is not unexpected: Wargan et al. (2010) showed that spatial patterns of tracer fields in constituent data assimilation are controlled mainly by the model dynamics, which is the same in both experiments. Figure 9c shows differences between the two analyses. Also shown are 10% difference contours. The differences are mostly within 1 ppmv. On 15 December and 15 January, the OMPS-LP analysis is on average the lower one of the two with the exception of the inner vortex on 15 January where the OMPS-LP analysis produces over 10% higher values. As that region is not illuminated by sunlight it is unconstrained by OMPS-LP or OMI observations but it is observed by MLS. Consequently, the large differences reflect a bias in the StratChem model with respect to MLS. On 15

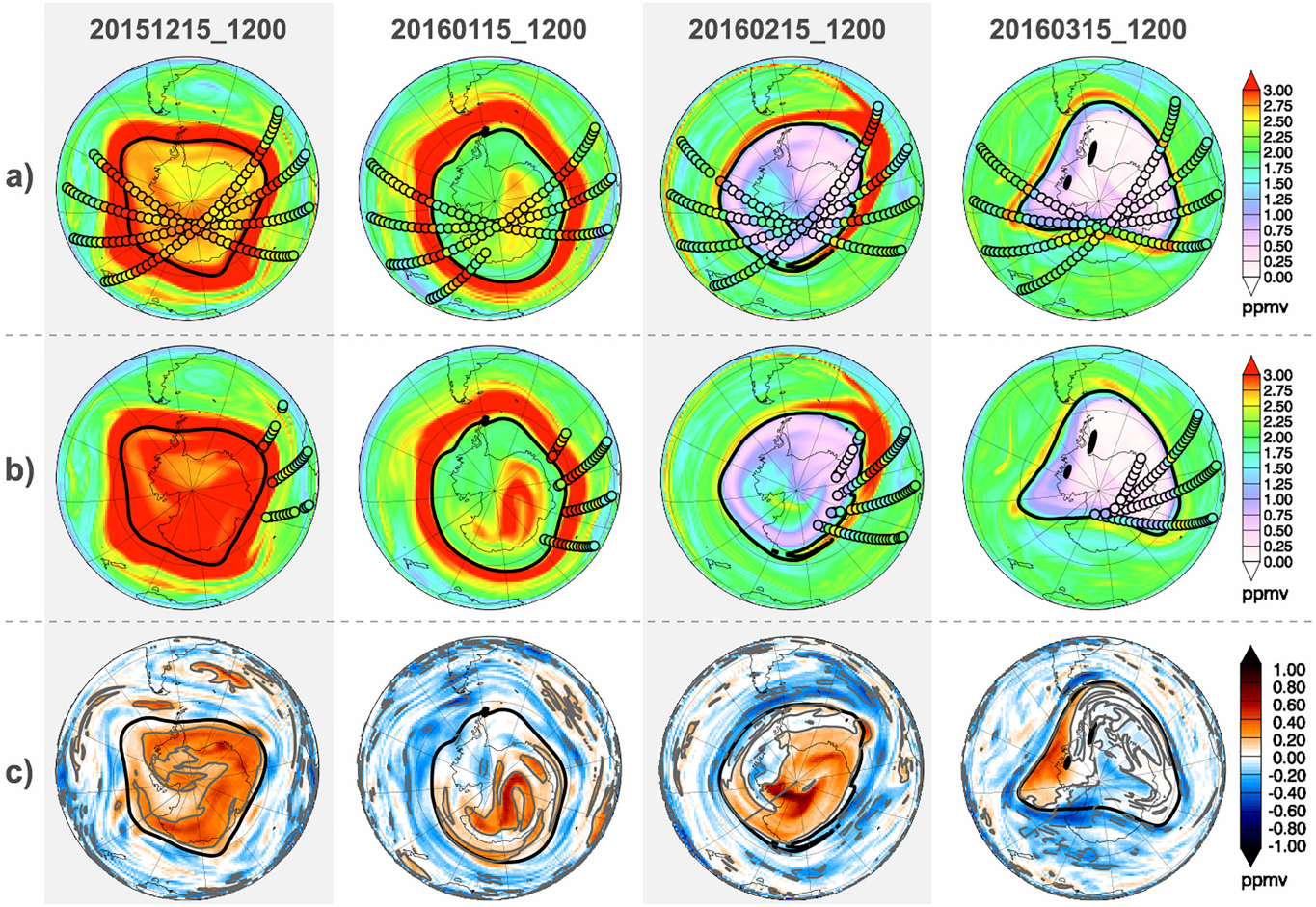

Figure 10. As in Figure 9 but for the austral winter-spring.

February and 15 March, the differences between the two experiments are smaller and less structured with a smaller area covered by differences in excess of 10%. However, the mixing ratio within the smaller vortex fragment is over 10% higher in the OMPS-LP analysis than in the MLS experiment. We note that there is no evidence of the difference patterns being aligned with the vortex edge. This is an important point because the use of a one-dimensional retrieval algorithm for OMPS-LP raises a question whether large ozone gradients are underestimated.

Also shown in Figure 9 are MLS and (adjusted) OMPS-LP observations collected within 6-hourly windows around the times of the analyses and interpolated to the 480-K theta surface using the MERRA-2 temperature. As expected, the analyses agree very well with the observations they assimilate (the circles look almost transparent against the background of the analysis fields). These plots also illustrate an important aspect of data assimilation: its ability to derive well resolved instantaneous global ozone fields based on a limited number of observations available at any given time.

3.4.2. The 2016 Ozone Hole

The 2016 ozone hole was average in size compared to other winters during the last decade (https://ozonewatch.gsfc.nasa.gov). It began to form in August and ended with a somewhat early final warming in mid-November. Figure 10 shows ozone maps at the 480-K potential temperature surface on 15 July, 15 August, 15 September, and 15 October illustrating the development of the ozone hole, analogous to Figure 9. The July ozone concentrations were high within the polar vortex as expected from climatology. By mid-August heterogeneous ozone loss has commenced within the outer portion of the vortex, leaving a high-ozone collar around the vortex edge. The depletion continued through September and October. On 15 October the vortex at 480-K isentrope was almost completely depleted of ozone with mixing ratios near zero over parts of West

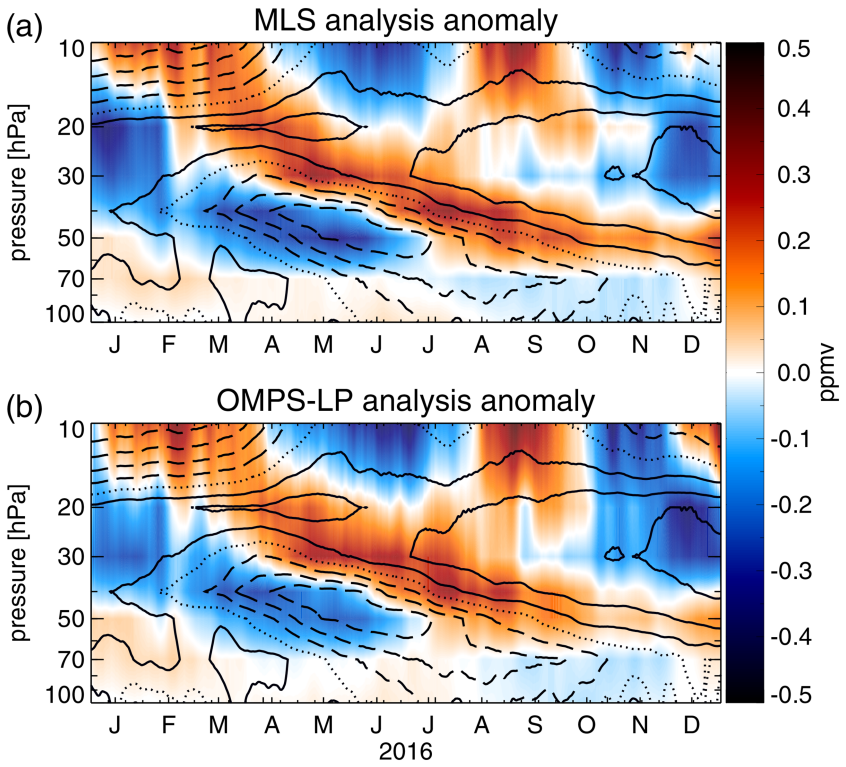

Figure 11. Deseasonalized ozone mixing ratio anomalies averaged between 5°S and 5°N (shaded) as a function of time and pressure for the MLS analysis (a) and OMPS-LP analysis (b). The black contours show the zonal wind in the same latitude band with contour intervals of 5 m/s. negative, zero, and positive wind speeds are shown as dashed, dotted, and solid lines, respectively. The plots were generated from 3-hourly analysis output with 5-day smoothing applied.

Antarctica and the Southern Ocean. As was the case of the boreal winter, the morphology of the ozone fields is similar between the two experiments but there are some notable differences in mixing ratios. The July polar vortex ozone is higher in the OMPS-LP analysis by 10% and more. In August, the OMPS-LP experiment still shows higher values in the inner portion of the vortex but slightly lower mixing ratios in the outer part where ozone depletion by active chlorine had already started. As the vortex was almost entirely unobserved by OMPS-LP in both months, these differences reflect the model bias with respect to MLS rather than a relative bias between the two instruments. The differences are within 1 ppmv. While that translates into large percent values inside the vortex in September and October due to the fact that the ozone concentrations are close to zero, the absolute (very low) values of mixing ratios are similar between the two analyses.

In September and October, the OMPS-LP analysis shows a weaker ozone gradient across the vortex edge compared to the MLS experiment, unlike in the case of the Arctic winter. Note that the edge is observed by OMPS-LP in both months. Because the OMPS-LP ozone algorithm does not account for horizontal inhomogeneity in ozone distribution this results in the weaker gradient as the instrument's line of sight intersects the vortex edge and the measured radiances, nominally originating from a tangent point inside the vortex also contain information from the region between the edge and the sensor, where ozone is much higher. This leads to an overestimation of the low concentrations inside the vortex and an underestimation of the high values immediately outside of it. This effect is seen at all theta levels between 400 and 500 K. Here, we note several important points. First, this effect does not change the main features of the ozone field: A high-ozone collar around the vortex edge and a sharp gradient across the edge are present in both analyses. Second, it would be instructive, in a future study, to compare these results with an assimilation of OMPS-LP ozone retrieved using the tomographic approach of Zawada et al. (2018). That study demonstrates that their two-dimensional algorithm resolves the ozone gradients better than the one-dimensional version used here. However, it should be noted that the differences in the representation of the ozone gradients across the vortex edge between different retrieval algorithms do not affect the ability of assimilation to reproduce long-term ozone variability.

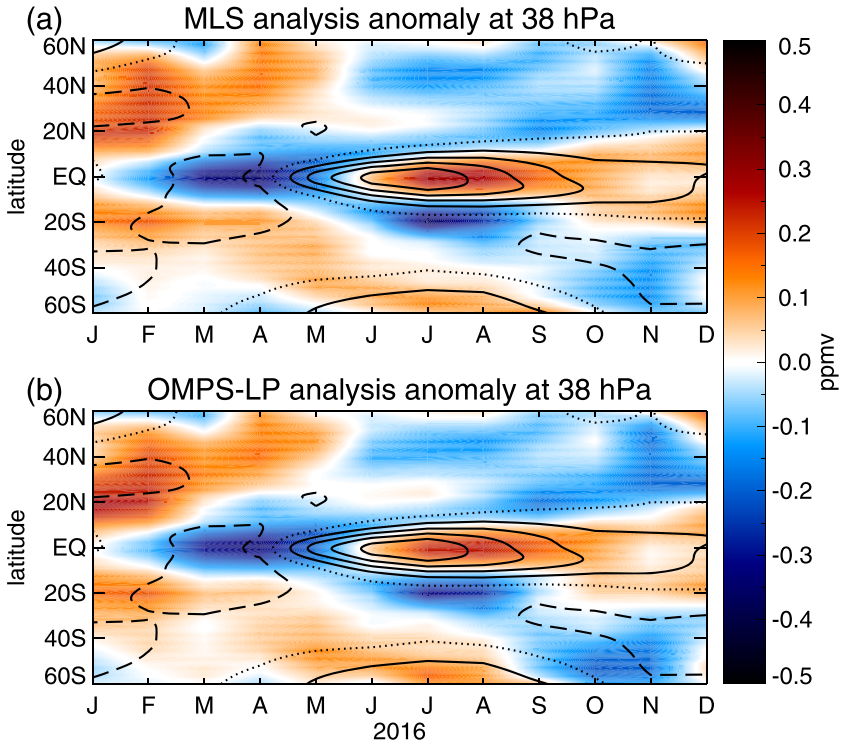

Figure 12. Deseasonalized monthly ozone mixing ratio anomalies at the 38-hPa pressure level as a function of month and latitude (shaded) and vertical shear of the zonal wind (contours) for the MLS analysis (a) and OMPS-LP analysis (b). The interval of the shear contours is 0.002 s^{-1}. Negative, zero, and positive shear values are shown as dashed, dotted, and solid lines, respectively.

3.4.3. The QBO Disruption

The QBO is a major mode of dynamical variability of the stratosphere and one that strongly affects tropical ozone via transport below ~30 km, and through a combination of transport and chemistry in the middle and upper stratosphere (Chipperfield et al., 1994; Logan et al., 2003). In the lower stratosphere, descending westerly wind shear layers induce anomalous downwelling in the tropics that acts on the strong vertical ozone gradient there, leading to positive concentration anomalies. The opposite occurs for easterly wind shears. Extratropical lower stratospheric ozone is also affected by a secondary meridional circulation induced by the QBO (Gray & Pyle, 1989) producing an out-of-phase relationship between the tropical and extratropical ozone anomalies. In the beginning of 2016 an anomalously high Rossby wave momentum flux into the tropics led to an upward displacement of a descending zone of westerly winds, accompanied by a downward propagating region of easterlies (Coy et al., 2017; Newman et al., 2016; Osprey et al., 2016). This disruption strongly affected tracer transport in the lower stratosphere (Tweedy et al., 2017).

The evolution of the 5°S to 5°N averaged deseasonalized ozone partial pressure anomalies from the MLS and OMPS-LP analyses along with the zonal mean zonal wind is shown in Figure 11 as a function of pressure. The ozone anomalies were computed by removing the monthly mean MERRA-2 climatology from each analysis and then recentering the result around zero at every level. The MLS and OMPS-LP analyses produce almost identical anomaly patterns consistent with our understanding of tropical ozone transport due to the QBO. Evident is a region of descending negative anomalies between January and June coincident with the region of anomalous easterlies at pressures between 20 and 70 hPa. This is followed by a layer of positive anomalies aligned with the westerly wind shear starting at about 30 hPa in March and continuing through the rest of 2016. Figure 12 shows deseasonalized monthly ozone anomalies and vertical wind shear at 38 hPa as a function of time and latitude, similar to Figure 3 of Tweedy et al. (2017). In agreement with that study, the tropical ozone anomalies change from negative to positive in June, about 1 month before the positive wind shear attains a maximum. An opposite change occurs in the extratropics, indicative of the anomalous meridional circulation induced by the QBO disruption. The minimum ozone anomaly is seen around 20°S in

July and August, again consistent with the results reported by Tweedy et al. (2017). Here, as well as at other pressure levels in the lower stratosphere (not shown), a remarkable agreement between the results of the two analyses is evident.

These results highlight the ability of limb ozone assimilation to represent the ozone responses to the QBO correctly, as previously demonstrated for MLS (Coy et al., 2016). This is in contrast to a number of reanalyses that assimilate layer ozone from nadir Solar Backscatter UltraViolet radiometers (SBUV) but not limb observations, for example, MERRA-2 prior to 2004: due to large vertical smoothing errors inherent in ozone data derived from nadir observations (Kramarova et al., 2013) the downward phase propagation of the ozone QBO signal in these reanalyses is often poorly represented (Davis et al., 2017, their Figure 8; Coy et al., 2016).

4. Conclusions

An evaluation was presented of the relative performance of MLS and OMPS-LP ozone assimilation, focusing on the aspects relevant to a continuity of ozone record in future reanalyses. A simple adjustment scheme was applied to the OMPS-LP data by removing the zonal mean monthly differences from MLS for UV and Vis observations separately. Two assimilation experiments were performed for the year 2016 using a version of the GEOS data assimilation system with the full stratospheric chemistry model, StratChem, and driven by the MERRA-2 meteorology. These experiments are constrained by stratospheric ozone profiles from MLS and OMPS-LP, respectively, and are set up identically otherwise. The main results are summarized as follows.

1. In the middle and upper stratosphere, the two analyses agree very well, with the mean differences within 3% and difference standard deviations within 10%. Larger differences are seen in the lower stratosphere, particularly in the Tropics.
2. The two analyses exhibit extremely similar difference patterns against independent observations from ozonesondes and ACE-FTS. The only large discrepancy is seen at 100 hPa over the Central Pacific between January and April of 2016, that coincides with the strong El Niño event. This discrepancy is subject to ongoing investigation.
3. Heterogeneous ozone depletion during polar spring is realistically represented in both analyses. The largest differences of 10–20% are confined to the interior of the polar vortex during summer months where there are no observations from OMPS-LP. The ozone gradient across the vortex edge in the Southern Hemisphere spring is less sharp in the OMPS-LP analysis than in the MLS experiment. This is an expected effect in OMPS-LP retrievals because the algorithm does not account for inhomogeneity along the sensor's line of sight.
4. Ozone transport during the 2016 QBO disruption event is represented very well in both experiments and in excellent agreement with other studies.

Although not shown here, the results of combined assimilation of MLS, OMPS-LP, and OMI fall between those of the MLS and OMPS-LP experiments, which are already in close agreement. An important consequence of this is that the two types of limb data can be assimilated separately or jointly without affecting the quality of the analyses significantly, at least outside of the polar night, providing a redundancy needed when data from one of the sensors become unavailable either due to a temporary outage or permanently.

Overall, the largest differences between the two analyses evaluated here are confined mainly to (1) the regions where OMPS-LP does not collect data: polar night and at pressures greater than 200 hPa, (2) the equatorial Pacific at the tropopause, and (3) the tropical lower stratosphere in general, due to the oscillations in the MLS profiles there. In most of the stratosphere the agreement is excellent in terms of both mean values and statistical distributions, providing a strong indication that even the simple adjustment scheme applied here will be sufficient to ensure continuity of the ozone record in future reanalyses that will use both these data sources. This result comes with a caveat: Kramarova et al. (2018) found that OMPS-LP exhibits a positive altitude-dependent drift with respect to other satellite data sets that are considered stable. The drift is generally within 1% per year but large enough to pose a problem for trend studies. Further work is required to fully understand and correct this issue.

The methodology discussed here can be extended to include future OMPS-LP sensors. Periods of overlap between different OMPS-LP instruments can be used for data adjustment if there are systematic

differences between them. Alternatively, one could explore the possibility of using solar occultation data or limb observations from the Optical Spectrograph and InfraRed Imager System (Llewellyn et al., 2004) as transfer standards for data homogenization of multiple limb sensors. A long-term stable data record such as from Optical Spectrograph and InfraRed Imager System would make it possible to produce homogenized data sets if gaps between consecutive future OMPS-LP missions arise, for example, due to sensor failures. Ozonesonde records can also be considered as transfer standards if long-term stability of these observations can be established.

Most modern multidecadal reanalyses to date have not used any type of bias correction of the ozone data they assimilate (Davis et al., 2017; Fujiwara et al., 2017). The latest reanalysis produced by the European Centre for Medium-Range Weather Forecasts, ERA5 is the first one to apply an adaptive bias correction algorithm to the assimilated ozone data but the results of this approach on the ERA5 ozone have not yet been evaluated in the published literature. The present study documents a first step toward generating a reanalysis suitable for long-term ozone monitoring of stratospheric ozone recovery in the 21st Century through combined assimilation of MLS and OMPS-LP data.

Acknowledgments
Resources supporting this work were provided by the NASA High-End Computing (HEC) Program through the NASA Center for Climate Simulation (NCCS) at Goddard Space Flight Center. MERRA-2 is an official product of the Global Modeling and Assimilation Office at NASA GSFC, supported by NASA's Modeling, Analysis and Prediction (MAP) program. We thank the World Ozone and Ultraviolet Radiation Data Centre (WOUDC, https://woudc.org) and the Southern Hemisphere Additional Ozonesondes (SHADOZ, https://tropo.gsfc.nasa.gov/shadoz/) for providing the ozonesonde data. The Atmospheric Chemistry Experiment (ACE), also known as SCISAT, is a Canadian-led mission mainly supported by the Canadian Space Agency. ACE-FTS data were downloaded from this site (http://www.ace.uwaterloo.ca/data.php). The output of the two analysis experiments discussed in this study can be made available on request. We thank three anonymous reviewers whose insightful comments on the original manuscript helped us significantly improve this study.

References

Ball, W. T., Alsing, J., Mortlock, D. J., Staehelin, J., Haigh, J. D., Peter, T., et al. (2018). Evidence for a continuous decline in lower stratospheric ozone offsetting ozone layer recovery. *Atmospheric Chemistry and Physics*, *18*(2), 1379–1394. https://doi.org/10.5194/acp-18-1379-2018

Ball, W. T., Alsing, J., Staehelin, J., Davis, S. M., Froidevaux, L., & Peter, T. (2019). Stratospheric ozone trends for 1985–2018: Sensitivity to recent large variability. *Atmospheric Chemistry and Physics*, *19*, 12,731–12,748. https://doi.org/10.5194/acp-19-12731-2019

Bernath, P. F., McElroy, C. T., Abrams, M. C., Boone, C. D., Butler, M., Camy-Peyret, et al. 2005). Atmospheric chemistry experiment (ACE): Mission overview, *Geophysical Research Letters.*, *32*, L15S01, https://doi.org/10.1029/2005GL022386, 15, L15S01

Bloom, S., Takacs, L., DaSilva, A., & Ledvina, D. (1996). Data assimilation using incremental analysis updates. *Monthly Weather Review*, *124*(6), 1256–1271. https://doi.org/10.1175/1520-0493(1996)124<1256:DAUIAU>2.0.CO;2

Chen, Z., DeLand, M., & Bhartia, P. K. (2016). A new algorithm for detecting cloud height using OMPS/LP measurements. *Atmospheric Measurement Techniques*, *9*, 1239–1246. https://doi.org/10.5194/amt-9-1239-2016

Chipperfield, M. P., Gray, L. J., Kinnersley, J. S., & Zawodny, J. (1994). A two-dimensional model study of the QBO signal in SAGE II NO_2 and O_3. *Geophysical Research Letters*, *21*, 589–592.

Cohn, S. E. (1997). An introduction to estimation theory. *J. Meteor. Soc. Japan*, *75*, 257–288.

Considine, D. B., Douglass, A. R., Connell, P. S., Kinnison, D. E., & Rotman, D. A. (2000). A polar stratospheric cloud parameterization for the global modeling initiative three-dimensional model and its response to stratospheric aircraft. *Journal of Geophysical Research*, *105*, 3955–3974. https://doi.org/10.1029/1999JD900932

Considine, D. B., Kawa, S. R., Schoeberl, M. R., & Douglass, A. R. (2003). N_2O and NO_y observations in the 1999/2000 Arctic polar vortex: Implications for transport processes in a CTM. *Journal of Geophysical Research*, *108*(D5), 4170. https://doi.org/10.1029/2002JD002525

Coy, L., Newman, P. A., Pawson, S., & Lait, L. R. (2017). Dynamics of the disrupted 2015/16 quasi-biennial oscillation. *Journal of Climate*, *30*(15), 5661–5674. https://doi.org/10.1175/JCLI-D-16-0663.1

Coy, L., Wargan, K., Molod, A. M., McCarty, W. R., & Pawson, S. (2016). Structure and dynamics of the quasi-biennial oscillation in MERRA-2. *Journal of Climate*, *29*(No14), 5339–5354. https://doi.org/10.1175/JCLI-D-15-0809.1

Davis, S. M., Hegglin, M. I., Fujiwara, M., Dragani, R., Harada, Y., Kobayashi, C., et al. (2017). Assessment of upper tropospheric and stratospheric water vapor and ozone in reanalyses as part of S-RIP. *Atmospheric Chemistry and Physics*, *17*, 12,743–12,778. https://doi.org/10.5194/acp-17-12743-2017

DeLand, M., Bhartia, P. K., Xu, P., & Zhu, T. (2017). OMPS limb profiler product O_3: Version 2.5 product description. Available from https://ozoneaq.gsfc.nasa.gov/media/docs/LP-L2-O3-DAILY_V2.5_Product_Description.pdf

Dhomse, S. S., Kinnison, D., Chipperfield, M. P., Salawitch, R. J., Cionni, I., Hegglin, M. L., et al. (2018). Estimates of ozone return dates from chemistry-climate model initiative simulations. *Atmospheric Chemistry and Physics*, *18*, 8409–8438. https://doi.org/10.5194/acp-18-8409-2018

Diallo, M., Riese, M., Birner, T., Konopka, P., Müller, R., Hegglin, M. I., et al. (2018). Response of stratospheric water vapor and ozone to the unusual timing of El Niño and the QBO disruption in 2015–2016. *Atmospheric Chemistry and Physics*, *18*, 13,055–13,073. https://doi.org/10.5194/acp-18-13055-2018

Douglass, A. R., Rood, R. B., Kawa, S. R., & Allen, D. J. (1997). A 3D simulation of the evolution of the middle latitude winter ozone in the middle stratosphere. *Journal of Geophysical Research*, *102*(D15), 19,217–19,232. https://doi.org/10.1029/97JD01043

Errera, Q., Chabrillat, S., Christophe, Y., Debosscher, J., Hubert, D., Lahoz, W., et al. (2019). Technical note: Reanalysis of Aura MLS chemical observations. *Atmospheric Chemistry and Physics*, *19*, 13,647–13,679. https://doi.org/10.5194/acp-19-13647-2019

Fang, X., Pyle, J. A., Chipperfield, M. P., Daniel, J. S., Park, S., & Prinn, R. G. (2019). Challenges for the recovery of the ozone layer. *Nature Geoscience*, *12*(8), 592–596. https://doi.org/10.1038/s41561-019-0422-7

Flynn, L. E., Seftor, C. J., Larsen, J. C., & Xu, P. (2006). The ozone mapping and profiler suite. In Qu, J. J. et al. (Eds.). *Earth science satellite remote sensing* (279–296). Berlin, Heidelberg: Springer. https://doi.org/10.1007/978-3-540-37293-6_15

Froidevaux, L., Jiang, Y. B., Lambert, A., Livesey, N. J., Read, W. G., Waters, J. W., et al. (2008). Validation of aura microwave limb sounder stratospheric ozone measurements. *Journal of Geophysical Research*, *113*(D15), *D15S20*. https://doi.org/10.1029/2007JD008771

Fujiwara, M., Wright, J. S., Manney, G. L., Gray, L. J., Anstey, J., Birner, T., et al. (2017). Introduction to the SPARC reanalysis Intercomparison project (S-RIP) and overview of the reanalysis systems. *Atmospheric Chemistry and Physics*, *17*, 1417–1452. https://doi.org/10.5194/acp-17-1417-2017 2017

Gelaro, R., McCarty, W., Suárez, M. J., Todling, R., Molod, A., Takacs, L., et al. (2017). The modern-era retrospective analysis for research and applications, version 2 (MERRA-2). *Journal of Climate*, *30*, 5419–5454. https://doi.org/10.1175/JCLI-D-16-0758.1

Gray, L., & Pyle, J. (1989). A two-dimensional model of the quasi-biennial oscillation of ozone. *Journal of the Atmospheric Sciences*, *46*, 203–220.

Hubert, D., Lambert, J.-C., Verhoelst, T., Granville, J., Keppens, A., Baray, J.-L., et al. (2016). Ground-based assessment of the bias and long-term stability of 14 limb and occultation ozone profile data records. *Atmospheric Measurement Techniques*, *9*(6), 2497–2534. https://doi.org/10.5194/amt-9-2497-2016

Kawa, S. R., Kumer, J. B., Douglass, A. R., Roche, A. E., Smith, S. E., Taylor, F. W., & Allen, D. J. (1995). Missing chemistry of reactive nitrogen in the upper stratospheric polar winter. *Geophysical Research Letters*, *22*, 2629–2632. https://doi.org/10.1029/95GL02336

Khosrawi, F., Kirner, O., Sinnhuber, B.-M., Johansson, S., Höpfner, M., Santee, M. L., et al. (2017). Denitrification, dehydration and ozone loss during the 2015/2016 Arctic winter, *Atmospheric Chemistry and Physics.*, *17*, 12,893–12,910, https://doi.org/10.5194/acp-17-12893-2017, 2017.

Kramarova, N. A., Bhartia, P. K., Frith, S. M., McPeters, R. D., & Stolarski, R. S. (2013). Interpreting SBUV smoothing errors: An example using the quasi-biennial oscillation. *Atmospheric Measurement Techniques*, *6*, 2089–2099. https://doi.org/10.5194/amt-6-2089-2013

Kramarova, N. A., Bhartia, P. K., Jaross, G., Moy, L., Xu, P., Chen, Z., et al. (2018). Validation of ozone profile retrievals derived from the OMPS LP version 2.5 algorithm against correlative satellite measurements. *Atmospheric Measurement Techniques*, *11*, 2837–2861. https://doi.org/10.5194/amt-11-2837-2018

Levelt, P. F., Joiner, J., Tamminen, J., Veefkind, J. P., Bhartia, P. K., Stein Zweers, D. C., Duncan, B., et al. (2018). The ozone monitoring instrument: Overview of 14 years in space. *Atmospheric Chemistry and Physics*, *18*, 5699–5745. https://doi.org/10.5194/acp-18-5699-2018

Levelt, P. F., van den Oord, G. H. J., Dobber, M. R., Mälkki, A., Visser, H., Vries, J. D., et al. (2006). The ozone monitoring instrument. *IEEE Transactions on Geoscience and Remote Sensing*, *44*, 1093–1101. https://doi.org/10.1109/TGRS.2006.872333

Livesey, N. J., Read, W. G., Wagner, P. A., Froidevaux, L., Lambert, A., Manney, G. L., et al. (2018). Version 4.2x level 2 data quality and description document. *JPL D-33509 Rev. D*, available from. https://mls.jpl.nasa.gov/data/v4-2_data_quality_document.pdf

Llewellyn, E. J., Lloyd, N. D., Degenstein, D. A., Gattinger, R. L., Petelina, S. V., Bourassa, A., et al. (2004). The OSIRIS instrument on the Odin spacecraft. *Canadian Journal of Physics*, *82*, 411–422. https://doi.org/10.1139/P04-005

Logan, J. A., Jones, D. B. A., Megretskaia, I. A., Oltmans, S. J., Johnson, B. J., Vömel, H., et al. (2003). Quasibiennial oscillation in tropical ozone as revealed by ozonesonde and satellite data. *Journal of Geophysical Research*, *108*(4244), D8. https://doi.org/10.1029/2002JD002170

Manney, G. L., & Lawrence, Z. D. (2016). The major stratospheric final warming in 2016, Dispersal of vortex air and termination of Arctic chemical ozone loss. *Atmospheric Chemistry and Physics*. https://doi.org/10.5194/acp-2016-633

Matthias, V., Dörnbrack, A., & Stober, G. (2016). The extraordinarily strong and cold polar vortex in the early northern winter 2015/2016. *Geophysical Research Letters*, *43*. https://doi.org/10.1002/2016GL071676

McPeters, R., Kroon, M., Labow, G., Brinksma, E., Balis, D., Petropavlovskikh, I., et al. (2008). Validation of the Aura ozone monitoring instrument total column ozone product. *Journal of Geophysical Research*, *113*, D15S14. https://doi.org/10.1029/2007JD008802

Meul, S., Dameris, M., Langematz, U., Abalichin, J., Kerschbaumer, A., Kubin, A., & Oberländer-Hayn, S. (2016). Impact of rising greenhouse gas concentrations on future tropical ozone and UV exposure. *Geophysical Research Letters*, *43*, 2919–2927. https://doi.org/10.1002/2016GL067997

Molod, A., Takacs, L., Suarez, M., & Bacmeister, J. (2015). Development of the GEOS-5 atmospheric general circulation model: Evolution from MERRA to MERRA2. *Geoscientific Model Development*, *8*, 1339–1356. https://doi.org/10.5194/gmd-8-1339-2015

Montzka, S. A., Dutton, G. S., Yu, P., Ray, E., Portmann, R. W., Daniel, J. S., et al. (2018). An unexpected and persistent increase in global emissions of ozone-depleting CFC-11. *Nature*, 2018, *557*(7705), 413. https://doi.org/10.1038/s41586-018-0106-2

Nash, E. R., Newman, P. A., Rosenfield, J. E., & Schoeberl, M. R. (1996). An objective determination of the polar vortex using Ertel's potential vorticity. *Journal of Geophysical Research*, *101*(D5), 9471–9478. https://doi.org/10.1029/96JD00066

Newman, P. A., Coy, L., Pawson, S., & Lait, L. R. (2016). The anomalous change in the QBO in 2015–2016. *Geophysical Research Letters*, *43*, 8791–8797. https://doi.org/10.1002/2016GL070373

Nielsen, J. E., Pawson, S., Molod, A., Auer, B., da Silva, A. M., Douglass, A. R., et al. (2017). Chemical mechanisms and their applications in the Goddard earth observing system (GEOS) earth system model. *Journal of Advances in Modeling Earth Systems*, *9*(8), 3019–3044. https://doi.org/10.1002/2017MS001011

Oman, L. D., Douglass, A. R., Salawitch, R. J., Canty, T. P., Ziemke, J. R., & Manyin, M. (2016). The effect of representing bromine from VSLS on the simulation and evolution of Antarctic ozone. *Geophysical Research Letters*, *43*(18), 9869–9876. https://doi.org/10.1002/2016GL070471

Orbe, C., Oman, L. D., Strahan, S. E., Waugh, D. W., Pawson, S., Takacs, L. L., & Molod, A. M. (2017). Large-scale atmospheric transport in GEOS replay simulations. *Journal of Advances in Modeling Earth Systems*, *9*. https://doi.org/10.1002/2017MS001053

Osprey, S. M., Butchart, N., Knight, J. R., Scaife, A. A., Hamilton, K., Anstey, J. A., et al. (2016). An unexpected disruption of the atmospheric quasi-biennial oscillation. *Science*, *353*(6306), 1424–1427. https://doi.org/10.1126/science.aah4156

Pawson, S., Stolarski, R. S., Douglass, A. R., Newman, P. A., Nielsen, J. E., Frith, S. M., & Gupta, M. L. (2008). Goddard earth observing system chemistry-climate model simulations of stratospheric ozone-temperature coupling between 1950 and 2005. *Journal of Geophysical Research*, *113*, D12103. https://doi.org/10.1029/2007JD009511

Purser, R. J., Wu, W.-S., Parrish, D. F., & Roberts, N. M. (2003). Numerical aspects of the application of recursive filters to variational statistical analysis. Part II: Spatially inhomogeneous and anisotropic general covariances. *Monthly Weather Review*, *131*, 1536–1548.

Randel, W. J., & Thompson, A. M. (2011). Interannual variability and trends in tropical ozone derived from SAGE II satellite data and SHADOZ ozonesondes. *Journal of Geophysical Research*, *116*, D07303. https://doi.org/10.1029/2010JD015195

Rault, D. F., & Loughman, R. P. (2013). The OMPS limb profiler environmental data record algorithm theoretical basis document and expected performance (2013). *IEEE T. Geosci. Remote Sens*, *51*, 2505–2527. https://doi.org/10.1109/TGRS.2012.2213093

Rochon, Y. J., Sitwell, M., & Cho, Y.-M. (2019). A study on harmonizing total ozone assimilation with multiple sensors. *Atmospheric Chemistry and Physics*, *19*, 9431–9451. https://doi.org/10.5194/acp-19-9431-2019

Sheese, P. E., Walker, K. A., Boone, C. D., Bernath, P. F., Froidevaux, L., Funke, B., et al. (2017). ACE-FTS ozone, water vapour, nitrous oxide, nitric acid, and carbon monoxide profile intercomparisons with MIPAS and MLS. *Journal of Quantitative Spectroscopy and Radiation Transfer*. https://doi.org/10.1016/j.jqsrt.2016.06.026

Simmons, A. J., Poli, P., Dee, D. P., Berrisford, P., Hersbach, H., Kobayashi, S., & Peubey, C. (2014). Estimating low-frequency variability and trends in atmospheric temperature using ERA-interim. *Quarterly Journal of the Royal Meteorological Society*, *140*(679), 329–353. https://doi.org/10.1002/qj.2317

Sofieva, V. F., Tamminen, J., Kyrölä, E., Mielonen, T., Veefkind, P., Hassler, B., & Bodeker, G. E. (2014). A novel tropopause-related climatology of ozone profiles. *Atmospheric Chemistry and Physics*, *14*(1), 283–299. https://doi.org/10.5194/acp-14-283-2014

SPARC/IO3C/GAW (2019) SPARC/IO3C/GAW report on long-term ozone trends and uncertainties in the stratosphere. I. Petropavlovskikh et al. (Eds.), SPARC Report No. 9, WCRP-17/2018, GAW Report No. 241, https://doi.org/10.17874/f899e57a20b, Retrievded from http://www.sparc-climate.org/publications/sparc-reports

Thompson, A. M., Witte, J. C., Sterling, C., Jordan, A., Johnson, B. J., Oltmans, S. J., et al. (2017). First reprocessing of southern hemisphere additional ozonesondes (SHADOZ) ozone profiles (1998–2016): 2. *Comparisons with satellites and ground-based instruments. Journal of Geophysical Research: Atmospheres*, *122*(13), 000–13,025. https://doi.org/10.1002/2017JD027406

Tweedy, O. V., Kramarova, N. A., Strahan, S. E., Newman, P. A., Coy, L., Randel, W. J., et al. (2017). Response of trace gases to the disrupted 2015–2016 quasi-biennial oscillation. *Atmospheric Chemistry and Physics*, *17*, 6813–6823. https://doi.org/10.5194/acp-17-6813-2017

Wargan, K., Labow, G., Frith, S., Pawson, S., Livesey, N., & Partyka, G. (2017). Evaluation of the ozone fields in NASA's MERRA-2 reanalysis. *Journal of Climate*, *30*, 2961–2988, https://doi.org/10.1175/JCLI-D-16-0699.1, No 8

Wargan, K., Orbe, C., Pawson, S., Ziemke, J. R., Oman, L. D., Olsen, M. A., et al. (2018). Recent decline in extratropical lower stratospheric ozone attributed to circulation changes. *Geophysical Research Letters*, *45*(10), 5166–5176. https://doi.org/10.1029/2018GL077406

Wargan, K., Pawson, S., Olsen, M. A., Witte, J. C., Douglass, A. R., Ziemke, J. R., et al. (2015). The global structure of upper troposphere-lower stratosphere ozone in GEOS-5: A multiyear assimilation of EOS Aura data. *Journal of Geophysical Research – Atmospheres*, *120*, 2013–2036. https://doi.org/10.1002/2014JD022493

Wargan, K., Pawson, S., Stajner, I., & Thouret, V. (2010). Spatial structure of assimilated ozone in the upper troposphere and lower stratosphere. *Journal of Geophysical Research*, *115*, D24316. https://doi.org/10.1029/2010JD013941

Waters, J. W., Froidevaux, L., Harwood, R. S., Jarnot, R. F., Pickett, H. M., Read, W. G., et al. (2006). The earth observing system microwave limb sounder (EOS MLS) on the Aura satellite. *IEEE Transactions on Geoscience and Remote Sensing*, *44*, 1075–1092.

Witte, J. C., Thompson, A. M., Smit, H. G. J., Fujiwara, M., Posny, F., Coetzee, G. J. R., et al. (2017). First reprocessing of southern hemisphere ADditional OZonesondes (SHADOZ) profile records (1998-2015): 1. *Methodology and evaluation. J. Geophys. Res. Atmos.*, *122*, 6611–6636. https://doi.org/10.1002/2016JD026403

Witte, J. C., Thompson, A. M., Smit, H. G. J., Vömel, H., Posny, F., & Stübi, R. (2018). First reprocessing of Southern Hemisphere ADditional OZonesondes profile records: 3. Uncertainty in ozone profile and total column. J. Geoph. Res.: Atmospheres, 123, 3243–3268. https://doi.org/10.1002/2017JD027791

WMO (World Meteorological Organization) (2018). Scientific assessment of ozone depletion: 2018. *Global Ozone Research and Monitoring Project*–Report No. 58, 588 pp., Geneva, Switzerland.

WMO-GAW/WOUDC (World Meteorological Organization-Global Atmosphere Watch Program/World Ozone and Ultraviolet Radiation Data Centre) ozonesonde data. Retrieved February 2017, from https://woudc.org. https://doi.org/10.14287/10000008

Wu, W.-S., Purser, R. J., & Parrish, D. F. (2002). Three-dimensional variational analysis with spatially inhomogeneous covariances. *Monthly Weather Review*, *130*, 2905–2916.

Zawada, D. J., Rieger, L. A., Bourassa, A. E., & Degenstein, D. A. (2018). Tomographic retrievals of ozone with the OMPS limb profiler: Algorithm description and preliminary results. *Atmospheric Measurement Techniques*, *11*, 2375–2393. https://doi.org/10.5194/amt-11-2375-2018